

Excitation of local magnetic moments by tunnelling electrons

Jean-Pierre Gauyacq^a, Nicolás Lorente^b, Frederico Dutilh Novaes^b

^a *Institut des Sciences Moléculaires d'Orsay, ISMO, Unité mixte CNRS-Université Paris-Sud, UMR 8214, Bâtiment 351, Université Paris-Sud, 91405 Orsay CEDEX, France*

^b *Centro de investigación en nanociencia y nanotecnología (CSIC - ICN), Campus de la UAB, E-08193 Bellaterra, Spain*

Abstract

The advent of milli-kelvin scanning tunneling microscopes (STM) with inbuilt magnetic fields has opened access to the study of magnetic phenomena with atomic resolution at surfaces. In the case of single atoms adsorbed on a surface, the existence of different magnetic energy levels localized on the adsorbate is due to the breaking of the rotational invariance of the adsorbate spin by the interaction with its environment, leading to energy terms in the meV range. These structures were revealed by STM experiments in IBM Almaden in the early 2000's for atomic adsorbates on CuN surfaces. The experiments consisted in the study of the changes in conductance caused by inelastic tunnelling of electrons (IETS, Inelastic Electron Tunnelling Spectroscopy). Manganese and Iron adatoms were shown to have different magnetic anisotropies induced by the substrate. More experiments by other groups followed up, showing that magnetic excitations could be detected in a variety of systems: e.g. complex organic molecules showed that their magnetic anisotropy was dependent on the molecular environment, piles of magnetic molecules showed that they interact via intermolecular exchange interaction, spin waves were excited on ferromagnetic surfaces and in Mn chains, and magnetic impurities have been analyzed on semiconductors. These experiments brought up some intriguing questions: the efficiency of magnetic excitations was very high, the excitations could or could not involve spin flip of the exciting electron and singular-like behavior was sometimes found at the excitation thresholds. These facts called for extended theoretical analysis; perturbation theories, sudden-approximation approaches and a strong coupling scheme successfully explained most of the magnetic inelastic

processes. In addition, many-body approaches were also used to decipher the interplay between inelastic processes and the Kondo effect. Spin torque transfer has been shown to be effective in changing spin orientations of an adsorbate in theoretical works, and soon after it was shown experimentally. More recently, the previously mentioned strong coupling approach was extended to treat the excitation of spin waves in atomic chains and the ubiquitous role of electron-hole pair creation in de-exciting spins on surfaces has been analyzed. This review article expounds these works, presenting the theoretical approach by the authors while trying to thoroughly review parallel theoretical and experimental works.

Keywords: IETS, magnetism, spin flip, MAE, magnetic anisotropy, spin-orbit coupling, scanning tunneling microscope, STM, inelastic effects, conductance, electron transport, spectroscopy, magnetic adsorbates, lifetimes, Kondo effect

1. Introduction

Tunneling phenomena is a purely quantal phenomena with great impact in current basic and applied research. The advent of solid-state devices led to the study of electron tunneling through insulating barriers in order to create a plethora of device designs based on electron tunneling [1]. From the fundamental point of view, tunneling offered many interesting phenomena and applications from imaging of surface structure and topography [2] to Josephson effect [3] and to inelastic electron tunneling spectroscopy (IETS) [4].

Inelastic electron tunneling spectroscopy was discovered when studying electron tunneling through an insulating thin film between two metallic electrodes. Jacklevic and Lambe [4] recorded differential conductance traces where a rich structure appeared at certain well-defined voltages. Their analysis led to the conclusion that they were measuring the change in conductance due to the excitation of vibrations of unknown impurities in the insulating layer. This finding led to the creation of a new type of spectroscopy, IETS, that was much developed in the 70's and 80's. Hansma [5] summarizes in a very interesting review article many of the molecular species studied in this way in different types of tunneling barriers, and on-going research efforts are currently undertaken in the IETS of insulating layer interfaces [6].

The advent of the scanning tunneling microscope (STM) started the search of IETS in the tunneling junction of the STM [7]. The stakes were

high: on the one hand-side, STM would be able to detect the vibrational signatures of the species in the junction making it possible to develop a chemical sensitivity absent in the usual STM operational modes; on the other hand-side, the extreme local sensitivity of the STM would permit to have a single-molecule spectroscopy. Despite theoretical evaluations that IETS was within reach in STM [7, 8], experimental proof only came in 1998 when Stipe, Rezaei and Ho showed the vibrational IETS of a single acetylene molecule adsorbed on a Cu (100) surface [9]. There are excellent review articles that describe the physics and history of IETS with the STM [10, 11].

The sophistication of STM opens the possibility of addressing lower energy scales. Very low temperatures and extreme sensitivity equipment appear along the 90's. Once that vibrational IETS was proven with the STM, lower-energy excitations became available. In 2004, Heinrich and co-workers [12] showed that magnetic excitations on a single magnetic atom were detected using a milli-Kelvin STM with a built-in magnetic field. This seminal experiment has given rise to a lot of activity in magnetic IETS on the atomic scale.

Both vibrational and magnetic IETS consist in a measurable change of conductance due to an excitation of an atom, molecule or general atomic structure under the tip of an STM. Hence, the tunneling current is both the exciting and the measuring probe. This dual behavior of the tunneling current makes IETS a complex technique where a simple-minded picture is surely error prone. However, a first-order approximation of how the excitation of an atom or molecule changes the conductance can be easily found in terms of the opening of new conduction channels linked to the excited molecular states [4, 5], see Fig. 1. Indeed, when the tip-sample bias is larger than the excitation energy, the tunneling electron can cede part of its energy to the molecule and still end up in a state above the Fermi energy of the corresponding electrode, thus contributing to the tunnelling current as part of an inelastic current. For bias below this threshold, the tunneling current is just formed of elastic electrons. When the new channel opens at the bias matching the excitation energy, the tunneling current increases because it now contains elastic as well as inelastic electrons. This abrupt change in the current leads to a jump in the differential conductance, and to a peak in the second derivative of the current with respect to bias, centered about the excitation energy in eV.

As announced, the previous picture is simplistic and it does not take into account the complexities of the many-body character of the excitation

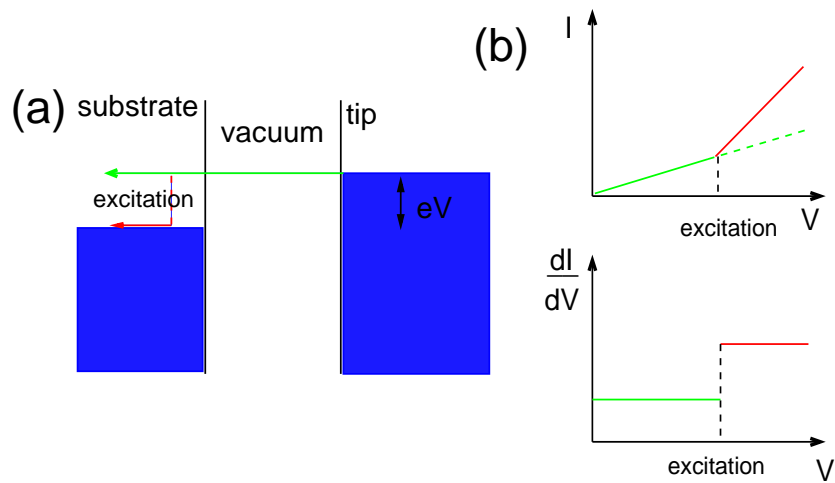


Figure 1: One-electron picture of the increase in conductance when an excitation takes place in the tunneling current. (a) Level scheme depicting the substrate and STM's tip electrodes as two metals with electron states filled up to the Fermi energy, which are respectively shifted by bias V times the electron charge e . Electrons can tunnel elastically (green trajectory) but also inelastically when the bias is larger than the excitation energy, because the inelastic trajectory proceeds above the substrate's Fermi energy (red trajectory). (b) The I - V characteristic is roughly linear with the bias. When the bias matches the excitation energy the inelastic channel becomes available. Hence the current increases. The lower panel shows the differential conductance behavior which is flat but presenting a discontinuity at the bias matching the excitation energy.

process. There are cases where the conductance decreases instead of increasing. This was shown by Hahn *et al.* [13] in the case of O₂ adsorbed on Ag (110) where the IETS shows dips instead of peaks. The study of this system showed that the appearance of dips can be associated with the mixed-valence electronic structure character of O₂ on Ag (110) [14].

A big difference between vibrational and magnetic IETS was quickly revealed. While vibrational IETS rarely implies increases of the conductance of more than 10%, magnetic IETS easily reaches 100% or more of change in conductance. This behavior can be traced back to the strengths of the interactions at play: while electron-vibration couplings are weak, electron-spin couplings are very large. The first consequence of this fact is that the perturbational approaches developed for vibrational IETS [8, 15, 16, 17, 18] are no longer valid. A second consequence is that multiple successive excitations are easily accessible in magnetic IETS [19] in the case of strong currents. Finally, vibrational IETS is very sensitive to the symmetry and to the particular system and thus, only a few modes are detectable which has led to the creation of propensity rules for mode analysis [20, 21]. Similarly, not all excited states in a magnetic system can be excited by a tunnelling electrons (see e.g. below the discussion on spin wave excitation in Heisenberg chains) and this can be easily rationalized in terms of angular momentum conservation and spin-coupling coefficients [22].

Magnetic IETS has not been confined to a small number of atomic systems, but it has also been extended to spinwave excitation [23] and itinerant magnetism [24]. Moreover, the use of spin-polarized STM has made a natural connection of magnetic excitations with spin torque of magnetic atomic systems. The reversal of the magnetization of atomic structures by the tunneling current has been shown on magnetic islands [25, 26] and also on single atoms both at the experimental [19] and theoretical [27, 28] levels.

Finally, magnetic IETS is intrinsically linked to the Kondo effect. Indeed, Kondo effect is induced by spin-flip transitions in an impurity induced by collisions with the substrate electrons; this is exactly the same process as the one at play in magnetic IETS and one can expect strong links between the two phenomena, as well as the possible emergence of many-body effects (Kondo-like effects) in magnetic IETS.

Hence, despite its short life, magnetic IETS is a well established technique that we will expound in the present article. First, we will review the main experimental results that have been briefly mentioned above, together with other results to give the reader a vision of the breadth of the field. Second, we

will review and explain the main theoretical approaches trying to emphasize the main features of magnetic IETS. Finally, we will conclude and try to outline some perspectives of this powerful technique.

2. Experimental Results

We will review the experimental work on magnetic IETS by considering particular systems and the physics explored in those systems rather than by proceeding in chronological order. We aim at presenting the experiments in such a way as their particular features are emphasized.

In order to achieve this we will first review the experiments performed on atomic adsorbates decoupled from the metallic substrate by an atom-thick insulating layer. The presence of a thin insulating layer between adsorbate and substrate effectively separates the two and leads to their partial decoupling, and thus to longer electronic lifetimes for states localised on the adsorbate. Experimental studies of these excited states become easier and better resolved and even spin lifetimes become measurable as we will present. Yet, IETS succeeded in revealing the presence of magnetic excitations for magnetic atoms adsorbed directly on a metallic substrate. Metallic substrate can also be magnetic, given rise to collective excitation such as magnons. We will also review these experiments. Other type of collective excitations can take place in chains of adsorbates as has been shown for artificially assembled Mn chains. Next, we will increase the complexity of IETS by studying the experiments performed with polarized electrons that naturally lead to spin torque and magnetization reversal. Finally, we will briefly mention experiments on magnetic IETS and Kondo physics.

2.1. Magnetic adsorbates partially decoupled from the metallic substrate

Heinrich and co-workers [12] showed for the first time that the STM could be used to create a magnetic excitation in an atomic adsorbate. The experiment was performed in ultra-high vacuum (UHV), at 0.6 K, and in the presence of a magnetic field. The system was an adsorbed manganese atom on two layers of alumina (Al_2O_3) on a crystalline substrate of nickel aluminum. With this setup, they measured the bias at which an inelastic channel opens and the tunneling conductance presents a well-determined step. They used a high magnetic field to orientate the manganese spin. The measured energy needed to flip the adatom spin can be evaluated as the Zeeman energy of a

simple local magnetic moment:

$$\Delta = g\mu_B B \tag{1}$$

where μ_B is the Borh magneton, B the magnetic field and g the gyromagnetic factor. Δ is a very small energy. For $B = 7$ T, $\Delta \approx 0.8$ meV. This can only be resolved if the temperature is in the milli-Kelvin range (presently 600 mK) and if the adatom is substantially decoupled from the electron-hole pair excitations of the substrates in order to have a well-defined excitation energy. This extended lifetime is achieved by decoupling the adatom from the substrate by an insulating film of Al_2O_3 .

The experiments measured Δ as a function of the applied magnetic field by measuring the bias at which a step was found in the STM conductance. From Eq. (1), the gyromagnetic factor g was found to vary between 1.88 and 2.01 depending on the location of the Mn atom on the Al_2O_3 island. This first magnetic IETS example showed that g depends on the local environment of the studied atom, hinting at the existence of local interactions influencing the adsorbed magnetic atom.

In the absence of a magnetic field, the magnetic excitations of a free Mn atom are in the range of eV, corresponding to typical values of the exchange energy in atoms. However, on a substrate, the measured energies of excitations in adsorbed magnetic atoms correspond well to the Zeeman splitting plus the surface imposed magnetic anisotropy. Hence, typical adsorbate magnetic excitations are in the range of meV rather than eV.

Further experiments by the same group [29] explored more systems, revealing MAE (Magnetic Anisotropy Energy) by magnetic IETS. Indeed, Mn on a monolayer of CuN on Cu(100), and Fe on CuN on Cu (100), show excitation energies in the meV range, which evidences the sizable MAE of these systems. Figure 2 is the conductance measurement for the Fe/CuN/Cu (100) as a function of applied bias for different magnetic fields. Let us briefly present how MAE determines the low-energy spectra revealed by magnetic IETS.

In iron-group atoms, the crystal-field splitting of the $2L+1$ levels (where L is the orbital quantum number) is much larger than the spin-orbit coupling, even for the above case of adsorbates on a CuN monolayer. This leads to the quenching of the orbital angular momentum, see for example [30], and to the use of the spin operator to determine the magnetic state of the adsorbate. The spin-orbit interaction couples the states split by the crystal

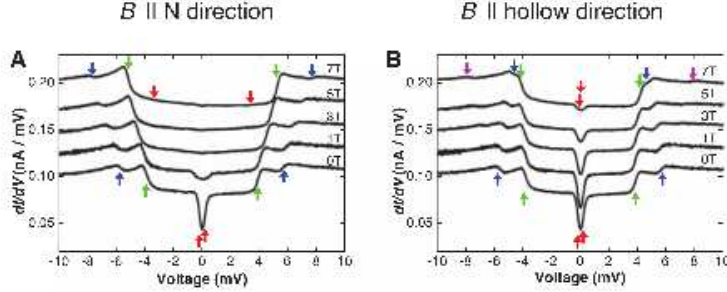


Figure 2: Conductance measurement for an STM junction on a Fe adatom on CuN/Cu(100), Ref. [29]. The Fe adatom is adsorbed atop a Cu atom. A magnetic B field is applied along two different directions parallel to the surface: a direction in the plane containing a Fe adsorbate and one of its first N neighbours ('N-direction') and the perpendicular direction ('hollow direction'). As a consequence of the anisotropic distribution of N neighbours around the Fe adsorbate, the magnetic structure of the Fe adsorbate shows a very clear anisotropy. It is revealed in the conductance spectrum when the external magnetic field is aligned along the *A* direction without or *B* with N atoms. The steps in the conductance take place at different energies stressing the magnetic anisotropy. From reference [29]. Reprinted with permission from AAAS.

field to higher lying states leading to second-order energy shifts of the states; it thus brings a coupling between the spin direction and its environment. The spin-orbit induced energy shifts can be represented by the effective spin Hamiltonian [30]:

$$\hat{H} = D\hat{S}_z^2 + E(\hat{S}_x^2 - \hat{S}_y^2). \quad (2)$$

The constants D and E depend on the spin-orbit coupling constant and the crystal-field split energy levels of the adatom. Hence, MAE is due to the effect of the environment on the adatom spin via the spin-orbit coupling. The diagonalization of Hamiltonian (2) leads to the actual spin states of the adsorbate and to the low-energy magnetic excitation energies.

Hirjibehedin and collaborators [29] measured the excitation energies of the above Fe/CuN/Cu(100) and Mn/CuN/Cu(100) systems. From these energies they extracted D and E , becoming the first measurement of MAE and of the anisotropy Hamiltonian (2) at the single-atom level.

They found $D = -1.55$ meV and $E = 0.31$ meV together with $g = 2.11$ for Fe and $D = -0.039$, $E = 0.007$ and $g = 1.90$ for adsorbed Mn. The eigenstates of Hamiltonian 2 can now be found and fully characterized the IETS. These eigenstates are given in Ref. [29] in terms of the free-atom spin.

It is very instructive to look at the composition of the anisotropy states, Table 1. The excitation from the ground state to the second excited state of Fe basically involves transitions from $S_z = \pm 2$ to $S_z = \pm 1$ hence we can say that the impinging electron has to flip its spin to produce the excitation since Fe spin changes in $|\Delta S_z| = 1$. However, excitations to the first excited level remains among the $|S_z| = 2$ components Hence, this transition does not involve a spin flip of the impinging electron. The mixture of spin states by the anisotropies modifies any selection rule based on the spin of the colliding electron [22]. We will further elaborate on this point in the theory section.

	$ 2, +2\rangle$	$ 2, +1\rangle$	$ 2, 0\rangle$	$ 2, -1\rangle$	$ 2, -2\rangle$
Ground state	0.697	0	-0.166	0	0.697
First excited	0.707	0	0	0	-0.707
Second excited	0	0.707	0	-0.707	0
Third excited	0	0.707	0	0.707	0
Fourth excited	0.117	0	0.986	0	0.117

Table 1: Coefficients of the spin states obtained after diagonalizing Hamiltonian Eq. (2) for a zero external magnetic field in the $S = 2$ manifold. The anisotropy due to the crystal field imposed by the surface mixes up the different S_z components. If an external magnetic field is turned on, a privileged direction is set, and the spin states increasingly resemble the free atom states under the Zeeman effect for larger magnetic fields. Taken from reference [29].

Similar experiments have also been performed on magnetic molecules. Tsukahara and coworkers [31] have measured magnetic IETS on a iron phthalocyanine molecule adsorbed on a Cu (110) with a single layer of oxide. Again, the oxide layer reduces the charge transfer from the metal substrate to the molecule and the molecule keeps much of its free molecule character. However, adsorption has the dramatic consequence of reversing the anisotropy sign. Indeed $D = 8.9$ meV in the gas phase [32, 33] and the study of the magnetic IETS leads the authors to a $D = -6.4$ meV value. The transversal anisotropy E is very small. Iron phthalocyanine is a $S = 1$ molecule. The ligand field splits the d -electron manifold of the Fe atom at the center of the molecule, Fig. 3, and the 6 electrons in the d -orbitals are now rearranged following the tetrahedral energy ordering of the split d -orbitals. As a consequence, two unpaired electrons lead to a total $S = 1$ in the molecule.

The effect of the substrate is very important in the final values of the MAE. The authors find two possible orientations of the molecule on the

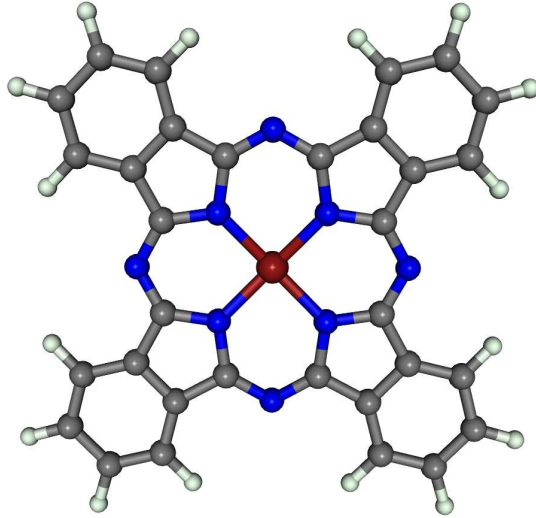


Figure 3: Ball-and-stick scheme of an iron phthalocyanine molecule. The central atom is the iron one, and the rest of atoms are nitrogen, carbon and hydrogen. The free molecule has a D_{4h} symmetry which is reduced upon adsorption. In the case of adsorption on the CuO/Cu(110) substrate [31], two different adsorption geometries are compatible, leading to different symmetries and to different MAE.

surface, leading to slightly different magnetic IETS and to different MAE values, this is clearly revealed under the effect of an external magnetic field. At zero magnetic field, the $S = 1$ electronic structure leads to a magnetic IETS showing only one step. This is because the strong D and zero E values split the $S = 1$ states into two levels of $|S_z| = 1$ and $S_z = 0$. Hence, there is only one possible excitation. The experimental inelastic change in conductance is $1/3$ of the total conductance. When the magnetic field is ramped up, the $|S_z| = 1$ levels split, and one more step appears in the magnetic IETS. Each of the two inelastic steps amount to 25% the elastic conductance. These values are characteristic of a $S = 1$ system [34, 35].

2.2. Lifetime measurements of adsorbate magnetic states

The existence of nano-magnets on a solid surface, the orientation of which could be changed at will by tunneling electrons, opens fascinating perspectives for the miniaturization of electronics. However, to lead to easily manageable devices, the excitation of local spins must have, among other properties, a sufficiently long lifetime. It is thus of paramount importance to

know the decay rate of the excited levels of the local spin and in particular to decipher the various parameters and effects that govern its magnitude.

The magnetic IETS experiments described above were performed in systems in which an insulating coating on the surface was separating the magnetic adsorbate carrying the local spin from the metal substrate. We will shortly review experiments on adsorbates directly deposited on a metallic substrate that do not lead to sharp IETS structures [36] as the above ones and this was attributed to a too short lifetime of the magnetic excitation on metals, stressing the importance of the decoupling layer between local spin and substrate in stabilizing the magnetic excitation.

De-excitation of a local spin implies energy transfer from the local spin to the substrate degrees of freedom, i.e. to the substrate electrons or phonons. Phonons are not directly coupled to spin variables, but only via spin-orbit couplings which make phonons particularly inefficient in the deexcitation process (see e.g. a discussion in [37]). In contrast, the adsorbate spin variables can be directly coupled to substrate electrons and electrons colliding on a magnetic adsorbate can easily induce magnetic transitions. Actually, this is exactly what happens in the magnetic excitation induced by tunneling electrons in the IETS experiments described above; in the de-excitation process the tunneling electrons are simply replaced by substrate electrons. The decay of excited magnetic states in individual adsorbates thus proceeds via electron-hole pair creation.

Recently, the decay rate of excited magnetic Mn atoms adsorbed on CuN/Cu(100) has been measured by Loth and collaborators [19] via the analysis of the dependence of the adsorbate conductivity on the tunneling current. By using magnetic inelastic excitation with a tunneling current, they changed the population of the different magnetic states. This can be actively achieved by varying the electron current. If the average time between tunneling electrons is shorter than the excited state lifetime, then the tunnelling electrons are probing partly excited adsorbates instead of probing only ground state adsorbates.

This multiple excitation has a dramatic effect on the tunneling conductance. Indeed, we have seen that an opening of an inelastic channel leads to a sharp change in the conductance. Once the channel is open, the conductance remains constant at low currents because the conduction conditions are unaltered. However at higher currents, the average time between tunneling electrons will start matching the excited state lifetime. As a result there will be tunneling electrons that probe the excited state instead of only the

ground state. The conductance of these excited states is different leading to a current dependent conductance. Moreover, as the bias increases, the number of inelastic electrons increase. Typically, in the Mn/CuN system studied by Loth et al [19] this leads to a drop of the conductance with bias after the first inelastic threshold is matched. The conductance vs bias curve presents a peak instead of step [19].

Loth and collaborators [19] modelled their experiment by using Pauli master equations or rate equations that consider the population evolution of the different magnetic states as a function of time depending on the excitation and deexcitation rates. From here they obtain that the typical spin lifetime of Mn on CuN/Cu(100) is in the sub-nano-second range. Moreover, the deexcitation rate depends on the energy of the excited state since the phase space for electron-hole pair excitation increases with the amount of available energy in the deexciting atom. Hence, they find that for example, at $B = 7$ T the longest lifetime is 0.25 ns for the first excited state, but it is 0.73 ns at $B = 3$ T meaning a smaller deexcitation rate as the excitation energy decreases.

The same group recently presented a more direct way of measuring the spin relaxation times [38]. They used an all-electronic pump-probe measurement scheme with an STM. A strong bias pulse first excites the magnetic atom and a second weaker pulse probes the excitation state of the same atom at a delayed time Δt . They studied the change in the number of detected electrons ΔN after the probe pulse compared to the number of tunneling electrons for the atom in its ground state. The number of electrons is obtained by integrating the measured current over Δt . The number of electrons in the ground state is obtained by integrating the current for a a probe pulse that precedes the pump pulse for a given large time (600 ns). They used a spin-polarized STM tip with its axis aligned with the studied atom. In the present case Fe on CuN/Cu(100). The excitation from the first electron pulse changes the alignment of the atom spin with respect to the tip's, implying a drop in the number of tunneling electrons. As the excited state decays, the number of electrons increases. Hence, ΔN is first negative and it goes exponentially to zero, since the current will match the elastic current at large time, Fig. 4. From this exponential decay, they obtained the excited state lifetime.

They increased the MAE of the adsorbed Fe atom by adding a nearby Cu atom. In this way, the first excitation energy was increased by a factor 4 as compared to the singly adsorbed Fe atom. As a consequence of the large

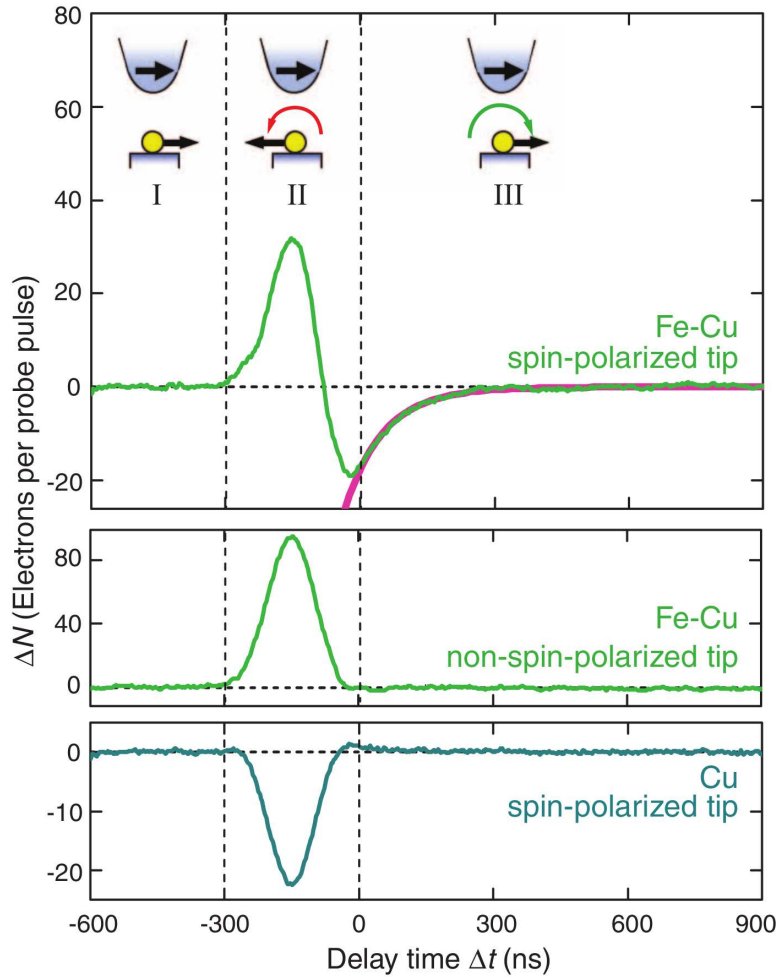


Figure 4: Pump-probe results with the STM. Here, the change in the number of detected electrons, ΔN , is measured as a function of the delay time. Experiments are performed under an external magnetic field of 7 T. In the region I, the probe pulse precedes the pump pulse. In the region II, the pump and probe pulses overlap, while in region III, the probe pulse follows the pump pulse. Insets depict the relative orientation of tip and sample spins. For the Fe-Cu dimer (top panel) ΔN decays exponentially in region III, with a spin relaxation time of 87 ns obtained from an exponential fit (magenta). Control experiments on the same Fe-Cu dimer but without spin sensitivity in the tip (middle panel) and on a Cu atom with spin-sensitivity in the tip (bottom panel). From reference [38]. Reprinted with permission from AAAS.

anisotropy, the measured spin lifetime was ~ 50 ns for $B = 1$ T, much larger than the relaxation times found for single Mn adsorbates.

These experiments show that an insulating layer and an important magnetic anisotropy leads to spin lifetimes in the ns range. However, when the magnetic atoms are directly adsorbed on a metal substrate the spin lifetime is greatly reduced [39]. More recent experiments [35] have measured a lifetime of 200 fs for the magnetic excitations of individual Fe atoms on Cu (111). The lifetime decreases by a factor of two when a magnetic field of 12 T is applied. The authors explained their findings by the decay of the magnetic excitation in substrate single-particle excitations or Stoner excitations where a spin-polarized electron-hole pair is produced.

2.3. Magnetic adsorbates on metallic substrates

Without a decoupling layer, a magnetic adsorbate on a metallic substrate is subject to a stronger hybridization and to a direct interaction with the continuum of electronic excitations of the metal. As we just saw, the first consequence is the shortened lifetime of adsorbate excitations due to the large probability of quenching the adsorbate excitation by exciting the metal substrate. The short lifetimes lead to an increased broadening of spectral features. Excitations are poorly resolved in energy and IETS in general becomes harder to detect on a metal surface.

Balashov and coworkers [36] succeeded to measure magnetic IETS on single Fe and Co adatoms on Pt (111). The inelastic signals were very small compared to the decoupled measurements shown above. In order to detect them, Balashov and coworkers [36] used the second derivative of the current with respect to bias, Fig. 5. This is in stark contrast to the measurements of Fe, Mn and Co on CuN/Cu (100), see Section 2.1, where the analysis of the first derivative was so clear that the use of the second derivative was not needed. The broadening caused by the coupling to the Pt (111) continuum of excitations is very large and of the order of the excitation energy itself, rendering the identification of the second derivative also difficult. Nevertheless, a careful statistical analysis permitted the authors to identify the excitation energies.

An extra difficulty in these experiments was the assignment of the measured peaks to magnetic excitations. The authors achieved it by excluding all other possible source of the detected peaks. The authors claimed that the peaks could not be assigned to collective excitations such as surface plasmons because they would then lie in the eV range. Vibrations are in the

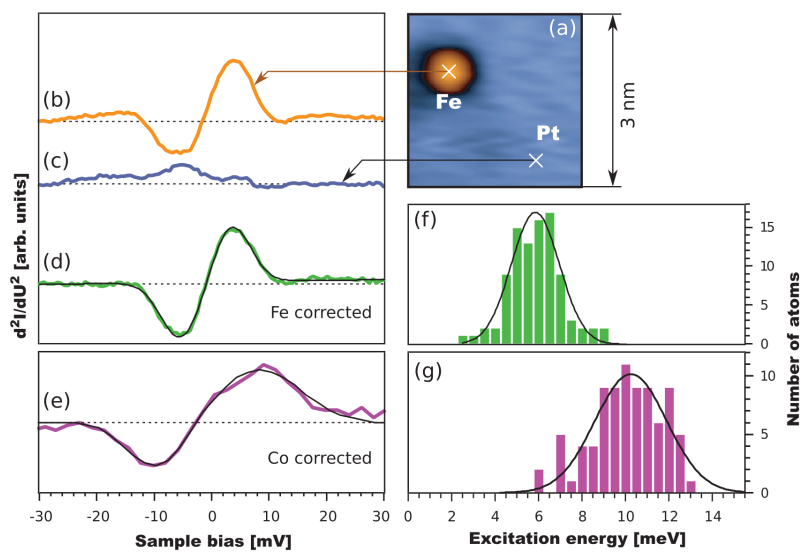


Figure 5: Magnetic IETS for a Fe atom adsorbed on a Pt (111) substrate [36]. (a) STM constant current image of a single Fe atom, (b) the second derivative of the current with respect to bias or IETS, (c) IETS of the bare Pt surface, (d) difference between (b) and (c). The same type of evaluation for a Co atom is shown in (e). (f) and (g) are the distributions of the measured energies for Fe and Co atoms respectively. Reprinted with permission from reference [36]. Copyright 2009 by the American Physical Society.

same energy range but the authors could not identify any with the measured peaks by doing a simple harmonic-approximation calculation within density functional theory. Finally, Kondo physics was left out of the possible causes because Fe and Co are known to give no Kondo peaks on Pt (111).

The probability of producing the magnetic excitation by the tunneling current was estimated to be in the range of 2% for both Fe and Co on Pt (111). The estimation was obtained by integrating the area of the second derivative peaks. However, due to the large broadening it is likely that part of the area is lost by overlapping of the negative and positive bias peaks, and hence 2% can be a very low lower limit of the inelastic efficiency. This IETS efficiency is typical of vibrational excitations [10, 11] and hence it is in strong contrast to the efficiencies measured for magnetic excitations of partially decoupled adsorbates, section 2.1, because they easily were larger than 100%. In these systems, several magnetic excitations were also easily detected. On a metal substrate this is probably impossible because the difference in energies are much smaller than the intrinsic broadening of the excitations.

Khajetoorians *et al* [24] have also measured the magnetic IETS of Fe adatoms, this time on Cu (111). In this case, the inelastic signal is directly seen in the conductance measurements. Two symmetric steps at negative and positive bias appear in the conductance. The step thresholds shift with the applied magnetic field, following an expected Zeeman splitting, section 2.1, showing unambiguously that these are magnetic excitations. The measured gyromagnetic factor g is 2.1, suggesting that the Fe adatom cannot be described by a pure spin. The step heights are 5%, again very small compared to the measured ones in the decoupled case, section 2.1.

As in the experiments by Balashov and coworkers [36], the broadening is very large. From the step broadening Khajetoorians *et al* [24] estimate a lifetime of 200 fs, orders of magnitude smaller than the decoupled case, section 2.1.

Khajetoorians and coworkers [24] also measured the adatom magnetic moment by using the single-atom magnetization curve (SAMC) technique [40]. They used an out-of-plane magnetized STM tip and measured the relative change in conductance with applied magnetic field. From these measurements they obtained that the Fe magnetic moment was $3.4 \mu_B$, quite different from the $4.0 \mu_B$ deduced in the IETS experiments of Fe on CuN / Cu(100) [29]. The value of the Fe magnetic moment is attributed to a consequence of the strong hybridization of the adatom with the metallic substrate. This led Khajetoorians and coworkers [24] to rationalize their findings in

terms of an itinerant spin model. This model shows that the lifetime limiting process of the magnetic excitations is their decay into electron-hole pairs, namely, Stoner excitations of the itinerant electron gas. This decay mechanism has also been modelled by Novaes and coworkers [28] albeit with a different formalism as we will review in the theory section.

2.4. Magnetic adsorbates on semiconducting substrates

A scenario for spin excitation different from the two seen above (magnetic impurities weakly coupled or strongly coupled to the substrate) is the case of magnetic impurities on a semiconducting surface. Despite the strong chemical interaction, the absence of conduction states in the semiconductor gap should lead to a strong charge localization on the impurity. In order to avoid this and to have some current, the substrates are weakly doped so that the system corresponds more to a decoupled one instead of a strongly coupled one.

Khajetoorians *et al* [35] have performed magnetic IETS experiments on Fe adatoms on indium antimonide, InSb (110). The samples are n-doped and the presence of a small Fe density leads to an accumulation layer on the surface and to the appearance of a two-dimensional electron gas (2DEG). This electron gas is characterized by only two electronic bands, one starting at -80 meV and the other one at -25 meV from the Fermi energy. Hence, in the present case, there is something like a surface metallic structure permitting the passage of the tunneling current from the STM tip.

The magnetic IETS are performed ontop of the Fe adatom and two clear steps, each amounting to 25% of the elastic conductance (hence 1/3 of the conductance is inelastic in the present case) at $V \approx \pm 0.5$ mV and $V \approx \pm 1.5$ mV. This very small energy scale comes from the small MAE as the authors found by fitting Eq. (2) to $D = -1.4$ meV and $E = 0.22$ meV.

In order to rationalize their experimental findings, the authors used the theory by Lorente and Gauyacq [22], see section 3, with the assumption that the electron transmission takes place through a unique electron-adatom spin coupling scheme. By analyzing the Landau levels of the 2DEG, they realized that the Fe adatom served as a spin filter and that indeed, only majority spins were contributing to the electron transmission (the same feature as that found in Ref. [22] for Fe on CuN/Cu(100)).

From their analysis, the authors conclude that the Fe spin on InSb (110) is a $S = 1$ system. This is clearly compatible with the three levels appearing from anisotropy split levels of $S = 1$. Furthermore, DFT calculations [35]

show that the Fe atomic configuration on the surface is rather $3d^84s^0$ than the free atom one $3d^64s^2$. The crystal field from the surface leads to the single population of two field-split d levels creating a $S = 1$ system in opposition to the $S = 2$ free atom as given by Hund's rules.

The 2DEG presents a rich Landau level structure when a magnetic field is applied. Analysis of the conductance of the Landau level structure is successfully exploited by the authors to measure the expectation value of the spin-component along the applied magnetic field. In particular, these measurement allowed the authors to identify the orientation of the easy axis and determined the anisotropy case unequivocally. Furthermore, the Landau levels leads to a spin splitting in the tunneling electrons, hence creating a spin-polarized electron source. Thanks to this spin polarization the authors could determine the spin-filtering effect of the Fe adatom.

This set of experiments is a compelling breakthrough in the use of magnetic impurities in semiconductors, particularly having in mind the possible application in spintronic devices that currently use semiconducting materials.

2.5. Collective excitations: magnetic surfaces

The excitation of localized spins partially decoupled from a metallic substrate, section 2.1, is very effective and yields large changes in conductance that are easily measured in an IETS experiment. As the coupling with the continuum of electronic excitations of the substrate is increased, the lifetime of the magnetic excitations is reduced and the magnetic IETS becomes a more difficult technique with smaller changes in conductance and very broadened features, section 2.3. However, there are other types of magnetic excitations than localized spins in an adatom. A magnetic substrate itself can have excitations, the above mentioned Stoner excitations are single-particle excitations. There are also collective excitations where the ensemble of spins of a substrate is excited. Magnetic substrates can hold waves where their spin change orientation in a concerted manner. These spin waves are called magnons when quantized for ferromagnetic materials.

The first measurement of magnons with magnetic IETS was reported by Balashov *et al* [23, 41]. They used the second derivative of the current with respect to bias to detect peaks when using a Fe (100) crystal and a Co thin film on Cu(111). On Fe (100) they detected a large peak of ~ 30 -mV width centered at 3.6 mV. They assigned this peak to the magnon excitation of Fe (100) with a large change of conductance of 27%.

In order to prove that this peak is indeed of magnetic origin, they used a spin-polarized tip and a magnetic field. The magnetic field was used to change the orientation of the Fe monocrystal. They showed that the peak height changed with the orientation of the Fe monocrystal. Magnon excitation entails a spin-flip, hence only minority-spin electrons from the tip are effected. From these facts, the author concluded that the large peak at 3.6 mV was indeed the magnetic IETS signal of magnon excitation in Fe (100).

Further experiments on Co thin films showed that the conductance linearly increases with the number of layers in the Co film. Using a phase-space argument, they concluded that this linear increase was a proof that the excitations were indeed of magnonic origin and not of phononic one since in this last case the excitations would extend into the Cu (111) substrate.

Collective excitations are also found on antiferromagnetic substrates, but they are more complex than the previous magnon excitations. Spin waves in antiferromagnetic layers of Mn on Cu₃Au (001) were measured by Gao *et al.* [42]. The second derivative spectra permitted them to extract the spin wave dispersion relation which is linear. The lifetime of the spin waves was seen to scale linearly with energy in agreement with neutron scattering measurements and theory, giving a compelling evidence for the excitation of spin waves in an antiferromagnetic substrate.

2.6. Collective excitations: chains of magnetic adsorbates

The atom manipulation capabilities of STM has permitted Hirjibehedin and coworkers [43] to assemble finite-size chains of Mn atoms on the CuN on Cu(100) substrate, Fig. 6. The magnetic properties of these structures were revealed using magnetic IETS. The Mn atoms in the chains are antiferromagnetically coupled. The analysis of the IETS spectra in terms of a simple Heisenberg chain permitted Hirjibehedin *et al* [43] to find the antiferromagnetic exchange coupling constant J to be 6.2 meV, varying by around 5% depending on the location of the chain in the CuN island. If instead of ontop Cu sites, the chain was built ontop of N sites, the J value was halved. The Mn atoms retained their free electron spin $S = 5/2$.

The excitation process revealed the magnetic structure of the full chain. This was again proven by comparing the IETS with the spin states appearing from the diagonalization of the Heisenberg chain Hamiltonian. Clear differences appear between chains with an even number of atoms and chains with an odd one. In the first case the ground state is $S = 0$, while odd chains have a finite total spin. This leads to a very different spectrum at low bias,

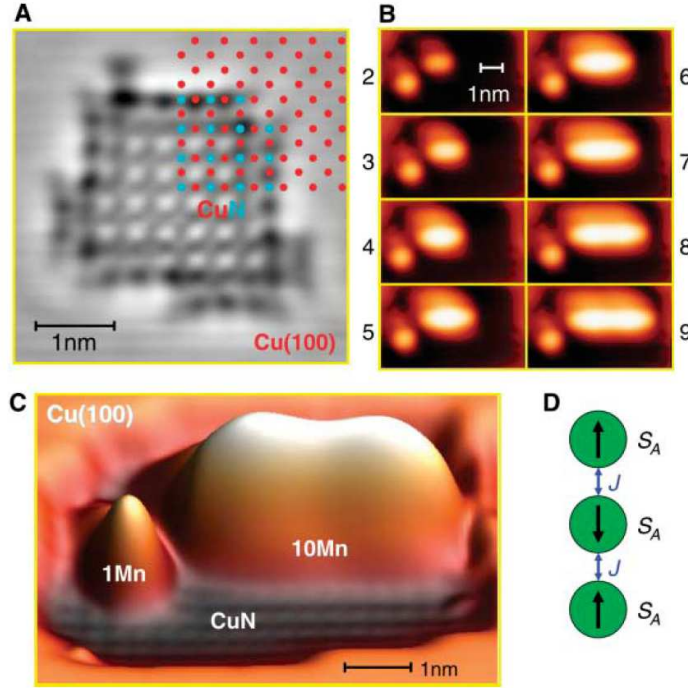


Figure 6: Chain of Mn adatoms on CuN/Cu(100) after Ref. [43]. In A, an STM constant-current image showing the substrate structure, B constant-current images of the different Mn chains and C a comparison of the different elements in the image. D shows a simple Heisenberg model that accounts for the exchange coupling among Mn atoms in the chain. From reference [43]. Reprinted with permission from AAAS.

even chains presenting a large elastic gap before the $S = 1$ channel becomes available. The triplet character of the first excited state in even chains was proved by splitting the conductance step in three steps in the presence of a magnetic field.

The many transitions available as the number of atoms in the chain changed, led the authors [43] to the conclusion that there were strict IETS selection rules. Indeed, the only peaks revealed in IETS were those corresponding to transitions $\Delta S = 0, \pm 1$ and $\Delta S_z = 0, \pm 1$. These selection rules can be easily explained by the spin-wave excitation model suggested by Gauyacq and Lorente [44] where the tunneling electron first flips the spin of a single Mn atom, and then the spin-flip propagates through the chain to build the actual excited state of the full system.

Recent density functional theory (DFT) calculations [45] show that Mn

chains on CuN/Cu(100) present a more complicated magnetic structure than just a first-neighbors Heisenberg chain. Indeed, the chain presents some spiral magnetic structure due to the appearance of non-negligible next-neighbors ferromagnetic couplings. From a classical spin Hamiltonian, the authors actually conclude that the Mn chains present weak ferromagnetism.

Another example of exchange-coupled magnetic chains was given in Ref. [46]. Instead of an atomically manipulated chain, the authors were studying the magnetic IETS of several molecular layers of cobalt phthalocyanine. This molecule replaces the Fe atom of Fig. 3 by a cobalt atom. The ligand field splitting leads to a d-electron configuration such that there is only one unpaired electron. Hence the molecule is a $S = 1/2$ system. The magnetic IETS shows however that the conductance spectrum changes as the number of molecular layers increases. The change in the IETS can be traced back to the magnetic interaction between molecules. Assuming a simple exchange interaction Heisenberg Hamiltonian, the fitting of two and three layer systems led to an exchange interaction, J , of 18 meV between molecules.

2.7. Polarized electrons: spin torque experiments

The capacity to controllably switch the magnetization of a magnetic adsorbate and, also, of a magnetic nanostructure is of great practical interest. Spintronic devices use spin-polarized currents to change and detect magnetic moments and in this way operate. In order to achieve this the spin-polarized current must exert a spin torque leading to the reversal of the local magnetization. Recently, it has been proved that it is possible to switch the magnetization of magnetic islands by using spin-polarized STM [25, 26].

Magnetic IETS is directly connected with spin torque experiments. Above we cited the experiment by Loth *et al.* [19] where they showed that by increasing the tunneling current they could multiply excite a magnetic adatom. The current gave them a natural time scale to calibrate the excited state lifetimes. Now, these excited states actually correspond to different directions of the atomic magnetization. Hence, by exciting the adatom, an effective spin torque was transferred from the tip to the substrate. In order to keep this new magnetization, the excited state must have a permanent and sizeable population which leads to large tunneling currents as compared with the electronic timestep fixed by the excited state lifetime, as we discussed above.

2.8. Magnetic IETS and Kondo physics

The Kondo effect is the screening of the spin of a magnetic impurity by the conduction electrons of a metallic substrate. The screening process involves a spin flip of the conduction electron at no energy cost. It is then an elastic spin flip. The Kondo effect is then intrinsically related to magnetic IETS. The signature of the Kondo effect in an STM experiment is the appearance of a zero-bias anomaly in the conductance spectra.

The ground state of the magnetic impurity has to be degenerate and differing in $\Delta S = 0, \pm 1$, $\Delta S_z = 0, \pm 1$ so that a spin flip takes from one state to the other degenerate state. However, magnetic anisotropy can lift the degeneracy preventing the formation of the Kondo state. Fractionary-spin impurities have at least a Kramers doublet [30] as ground state, hence even in the presence of an important MAE, the Kondo effect can take place. The Kramers doublet can be destroyed in the presence of a magnetic field. It is then interesting to follow the evolution of the Kondo effect with magnetic field.

Otte and coworkers [47] have shown the evolution of the conductance spectra with applied magnetic field in the case of a Co adatom on CuN/Cu(100), Fig. 7. At zero magnetic field, they retrieve a Kondo peak at zero bias. Due to the decoupling CuN layer, the Kondo temperature is very much reduced, from 54 K for the bare Cu (100) surface [48] to the measured 2.6 K [47]. This makes possible the observation of the Zeeman splitting of the Kondo peak at accessible magnetic fields.

In the same conductance spectra, magnetic IETS steps are found, which permits the determination of the parameters of Hamiltonian, Eq. (2), and hence, the energy structure of the different magnetic states. The fitting to the spectra yield a hard-axis ($D > 0$) anisotropy that favors the $S_z = \pm 1/2$ as the ground state. An easy-axis anisotropy would have given a $S_z = \pm 3/2$ doublet that are not linked via a spin-flip impeding the appearance of a Kondo effect. As the magnetic field is ramped up, the zero-bias anomaly splits to 2Δ , where Δ is given by Eq. (1). The rate at which the split peaks separate depends on the magnetic field direction as dictated by Hamiltonian (2).

This experiment shows that despite the breaking of the ground state degeneracy by the applied magnetic field, a remanent Kondo peak is found at the threshold of the spin-flip transition between $S_z = 1/2$ and $S_z = -1/2$ where the threshold is Δ , Eq. (1). Indeed, at threshold the two states are degenerate if one considers the total energy including the tunneling electron: it is the inelastic effect that connects via spin-flip the $S_z = 1/2$ and $S_z = -1/2$.

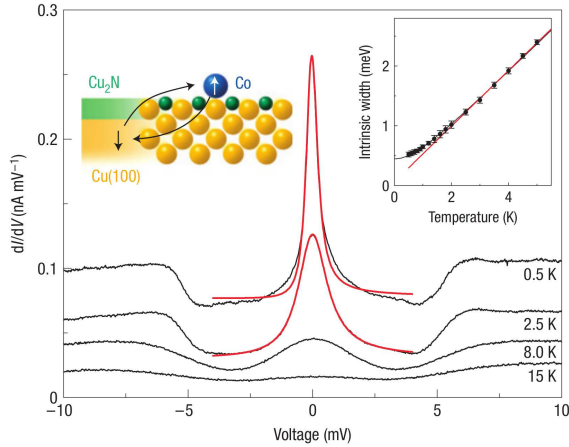


Figure 7: Conductance of an STM junction with a Co adatom on CuN/Cu(100). As the temperature is reduced, the zero-bias anomaly singles out and the inelastic steps are sharper. The inset shows the fit of the zero-bias peak width to the behavior of a the Kondo width evolution with temperature showing that the zero-bias anomaly is indeed a Kondo peak. Reprinted by permission from Macmillan Publishers Ltd: Nature Physics [47], copyright 2008.

Hence, there is a weak Kondo peak at threshold. This same behavior is to be expected at any threshold of spin-flip excitations. Indeed, recent theoretical work assign the spike-like features at the threshold of some magnetic IETS to these Kondo peaks [49]. They have evaluated the spectra of Fe and Co on CuN/Cu (100) and find some common features with the experiments [29, 47]. However, as shown by Loth and coworkers [19], the repeated excitation of the magnetic states as the tunneling current increases, also produces spikes at threshold. Moreover, Lorente and Gauyacq [22] (also see theory section 3) show that not all magnetic excitations in Fe on CuN/Cu(100) are spin flips. Hence, it is difficult to conclude on the extend of Kondo features in the above experimental spectra. A theoretical analysis of the Kondo effect at inelastic thresholds is presented in section 4.

However, clear Kondo features at the excitation threshold have been revealed for the singlet-triplet excitation of carbon nanotubes by an electron current [50]. These features have also been detected in the conductance spectra of a break junction containing C₆₀ molecules [51], and in cobalt complexes where the Kondo features have been modified via mechanical deformation of the molecule [52].

When an atom of Co is approached by a Fe atom on CuN/Cu(100) the above Kondo peaks is split by the exchange coupling between the adatoms [53]. When a magnetic field is applied on the sample, the ground and first excited states of Co can be made degenerate at $B \approx 2$ T in the experimental setup. This two levels differ in a spin-flip and they become degenerate at $B \approx 2$ T. As a consequence the full zero-bias anomaly is restored. The measured conductance spectrum is basically equal to the single Co one [53].

3. Theoretical results

3.1. Computation of magnetic anisotropy in adsorbates (*ab initio*)

The magnetic anisotropy of an isolated adsorbate on a surface is very often described using the effective anisotropy Hamiltonian (2) described in section 2.1 with the D and E anisotropy coefficients. It assumes the existence of a local spin, carried by the adsorbate, the direction of which is influenced by the surroundings. The origin of this effective Hamiltonian is described in detail in Ref [30] (see also descriptions of the magnetic anisotropy using tight-binding approaches in [54, 55, 56]). Briefly, in the case of a system with light atoms, the spin-orbit interaction can be considered to be weak, at least much weaker than the electrostatic interactions. In a calculation without spin-orbit interactions, the ground state is associated to a configuration of molecular (atomic) orbitals corresponding to a certain total spin of the adsorbate (\vec{S}^2) and degenerate with respect to the spin projection on the quantization axis (\hat{S}_z). Indeed, at this level of approximation, the adsorbate spin corresponds to the filling of the orbitals and does not interact with the adsorbate surroundings. The spin-orbit interaction can then be introduced as a perturbation that couples this ground state with excited states with different spin and orbital angular momenta. It leads to a second order correction on the energy, lifting the degeneracy of the ground state and splitting the different \hat{S}_z states. It can be stressed that, once the spin-orbit interaction is taken into account, the adsorbate states correspond to mixings of different spin and orbital angular momentum states and cannot, in principle, be labelled only considering \hat{S}_z . Though, if the spin-orbit perturbation is weak, the state mixing is weak, each state is dominated by a single \hat{S}_z value and one can keep the \hat{S}_z labelling of the different states as an approximation and represent the second order energy splitting of the ground state using Hamiltonian (2). The D and E parameters then describe the way the adsorbate magnetic moment orientates with respect to the substrate and they

are obtained by perturbation theory [30]. If a magnetic field, B , is applied, its action can be represented by a Zeeman term: $g\mu_B\vec{S} \cdot \vec{B}$, added to the Hamiltonian (2). μ_B is the Bohr magneton and g the Landé factor. Here again, one assumes that the states coming from the splitting of the ground state can be described by only considering S and possible extra mixings are introduced in the effective g factor.

Ab initio computation of the anisotropy coefficients (D and E coefficients for light adsorbates) then implies taking the spin-orbit interactions into account. Several calculations, based on Density Functional Theory (DFT), have been performed for adsorbates on different substrates that had been studied experimentally [45, 57, 58, 59, 60, 61, 62, 63, 64], a discussion of the assessment of the involved approximations can be found in Blonski and Hafner [65]. The DFT-based approach consists in introducing the spin-orbit as an operator involving the electron spin and added to the potential felt by the electrons [57, 66, 67, 68]. It is thus possible to compute the total energy of the adsorbate+substrate system for different orientations of adsorbate magnetic moments, this yields the magnetic anisotropy energy (MAE), or in other words, the magnetic landscape for the adsorbate. An adjustment procedure can then be used to extract the D and E coefficients that reproduce the computed MAE. Evaluation of the magnetic anisotropy thus involves making differences of total energies to get small energy terms. Typically for the case of Mn and Fe adsorbates on CuN/Cu(100) that have been studied experimentally by IETS [29], the magnetic anisotropy is in the meV energy range, so, a priori, it requires high accuracy calculations [57, 59]. This difficulty might account for the limited success of the *ab initio* evaluation of magnetic anisotropy terms in accurately accounting for IETS observations.

3.2. *Treatment of inelastic transitions induced by tunnelling electrons in a local spin*

The experimental observations of magnetic excitations by IETS that could be interpreted as magnetic transitions of a local spin in individual adsorbates prompted a series of theoretical studies, aiming at the understanding and description of the phenomena at play. The first accounts were considering one-electron approaches in which the tunnelling electron is directly inducing the transitions of the local spin.

3.2.1. S^2 theories

The first theoretical treatment of inelastic magnetic transitions accompanied one of the first experimental observations [29] of magnetic IETS. In IETS, the height of each step in the conductance corresponds to the strength of an inelastic transition, whereas the conductance at zero bias yields the elastic conductance. IETS thus yields a detailed account of the magnetic transitions induced by a tunnelling electron: the ratio between the zero-bias conductance and the conductance steps at finite bias yields the relative probability of elastic and inelastic scattering for a tunnelling electron with an energy larger than all inelastic thresholds. Starting from the anisotropy Hamiltonian (2), with a Zeeman term added, it is diagonalized in the basis set formed by the $|S, M\rangle$ states, the eigenstates of \vec{S}^2 and S_z , so that the anisotropy eigenstates can be written as:

$$|\phi_n\rangle = \sum_M C_{n,M} |S, M\rangle. \quad (3)$$

The ϕ_n eigenstate of the system is associated to the E_n eigenenergy. The steps in the conductance correspond to transitions from the ground state ϕ_1 to the excited ϕ_j states induced by the tunnelling electrons. By analogy with neutron scattering, the authors considered the \vec{S} operator as the transition operator and showed that the experimental ratio between the various inelastic channels could be very well accounted for by the ratio between the matrix elements squared of \vec{S} between initial, ϕ_1 , and final states, ϕ_j . This appears very clearly in Fig. 2 that shows the experimental and calculated tunneling conductance over a Fe atom on CuN/Cu(100) [29]. The S^2 scaling reproduces the ratio between inelastic channels; however, this scaling makes wrong predictions on the elastic channel and thus it cannot account for the overall strength of the magnetic transitions.

An extension of the original S^2 theory has been used in fitting procedures by Loth et al [69] and Chilian et al [70]. It consists in using a transmission amplitude equal to $(u + \vec{s} \cdot \vec{S})$, with u as an effective adjustable parameter. The u term only contributes to elastic tunnelling and added to the usual term of the original S^2 theory, it allows to fit the elastic channel at the desired level and thus to bypass the difficulty mentioned above about the original S^2 theory (vanishing u), which was unable to account for the elastic transmission.

Rationalization of the S^2 scaling was later provided within perturbation

theory approaches [71, 72]. The basic idea is to introduce in the Hamiltonian describing the tip-sample system a tunnelling term including the product of the electron spin times the adsorbate spin. Perturbation theory then allows to compute the current flowing through the tip and the adsorbate. This approach recovers the S^2 scaling for the excited channels, since the tunnelling term of the Hamiltonian contains the adsorbate spin as a factor. Its prediction is typical for a perturbative approach: the probability of the inelastic transition is proportional to the matrix element of the coupling between initial and final states. But it cannot make predictions on the elastic channel. This is not surprising for a process in which the inelastic transmission is dominating over the elastic one, perturbation theory cannot be expected to work.

Persson [73] went further in justifying the S^2 scaling. He made use of a sudden approximation (impulsive approximation) to treat tunnelling through the magnetic adsorbate. The magnetic anisotropy terms are very small and one can then assume that they are not active during electron tunnelling through the adsorbate, which is a very fast process in the absence of a very long-lived adsorbate-localised resonance. The electron tunnelling amplitude in the absence of magnetic anisotropy is expressed using Tersoff-Hamann [74] approximation taking into account the spin dependence of the T-matrix assuming complete spherical symmetry as justified by the sudden approximation. Then, the elastic and inelastic amplitudes are evaluated as the matrix element of the Tersoff-Hamann tunnelling amplitude between the initial and final states of the adsorbates, taking the anisotropy into account. In this way, the tunnelling current appears as the sum of two terms, one independent of the adsorbate spin variables and one proportional to the squared matrix element of the \vec{S} operator between initial and final states. This recovers the S^2 scaling of the inelastic channel probabilities without resorting to perturbation theory, but in the absence of a quantitative evaluation of the ratio between the two terms in the tunnelling current, it cannot make a quantitative prediction for the magnitude of the inelastic current with respect to the elastic current. Though, one can stress that the description of the relative importance of the various inelastic channels, irrespective of the elastic channel, by the so-called S^2 scaling is thus fully justified.

3.2.2. Strong coupling approach

A strong coupling theory has been developed for the magnetic IETS transitions; it is a one-electron approach that explicitly introduces the spin sym-

metries of the problem and leads to a simple formulation, allowing quantitative predictions on the strength of the elastic and inelastic channels [22, 34]. The effect of the anisotropy Hamiltonian (2) is treated in the sudden approximation, i.e. one defines a tunnelling amplitude between the tip and the substrate, noted $T_{Tip \rightarrow Sub}$ (and an equivalent one for the reverse tunnelling) without the anisotropy Hamiltonian terms taken into account. It corresponds to the tunnelling electron scattering from the adsorbate and it depends on the electron energy. In the absence of magnetic anisotropy (i.e. without spin-orbit interaction), it depends on the spin coupling between the tunnelling electron and the adsorbate, via the exchange interaction. Thus, it can be written in a diagonal form if we consider \vec{S}_T , the total spin of the (electron + adsorbate) system. Defining $|S_T, M_T\rangle$ as the eigenfunctions of \vec{S}_T^2 and $S_{T,z}$ (if S is the adsorbate spin, then $S_T = S \pm \frac{1}{2}$), we can write formally the scattering $T_{Tip \rightarrow Sub}$ matrix (in the absence of magnetic anisotropy) as:

$$T_{Tip \rightarrow Sub} = \sum_{S_T, M_T} |S_T, M_T\rangle T_{Tip \rightarrow Sub}^{S_T} \langle S_T, M_T|. \quad (4)$$

$T_{Tip \rightarrow Sub}^{S_T}$ is a complex number; it depends on the electron energy. However, the total span of bias that is considered in magnetic IETS is very small, so that $T_{Tip \rightarrow Sub}^{S_T}$ can be considered to be constant.

In the sudden approximation, the tunnelling amplitude (in the presence of magnetic anisotropy) is written as the matrix element of the $T_{Tip \rightarrow Sub}$ amplitude between the initial and final states of the tunnelling process. These states are written as $|\frac{1}{2}, m; \phi_n\rangle$ where the first part concerns the tunnelling electron (the electron spin is 1/2 and m is the projection of the tunnelling electron spin on the quantization axis) and the second part concerns the local spin of the adsorbate. One then obtains the amplitude, $AMP_{m,n \rightarrow m',n'}$, for a tunnelling electron induced transition from ϕ_n to $\phi_{n'}$, while the tunnelling electron spin projection changes from m to m' as:

$$AMP_{m,n \rightarrow m',n'} = \sum_{S_T} T_{Tip \rightarrow Sub}^{S_T} \times \sum_{M_T} \langle \frac{1}{2}, m'; \phi_{n'} | S_T, M_T \rangle \langle S_T, M_T | \frac{1}{2}, m; \phi_n \rangle \quad (5)$$

One can see that the tunnelling amplitudes associated to the two S_T symmetries are interfering. Equation (5) yields the transition amplitudes in the fully determined case, when the projection of the spin of the tunnelling electron is registered in both the initial and final states. Implicitly, it has been

assumed above that the tunnelling electron quantization axis is the z-axis of the adsorbate magnetic anisotropy; situations with different quantization axis for the adsorbate and the tunnelling electron can be easily handled with an expression similar to Eq. (5). We can now define the probability, $P_{n \rightarrow n'}$, for transitions from ϕ_n to $\phi_{n'}$ induced by unpolarized tunnelling electrons by summing incoherently over the distinguishable channels, as given by the tunneling electron's spin orientation m for the initial channel and m' for the final one:

$$\begin{aligned}
P_{n \rightarrow n'} &= \frac{1}{2} \sum_{m, m'} |AMP_{m, n \rightarrow m', n'}|^2 \\
&= \frac{1}{2} \sum_{m, m'} \left| \sum_{S_T} T_{Tip \rightarrow Sub}^{S_T} \right. \\
&\quad \times \left. \sum_{M_T} \langle \frac{1}{2}, m'; \phi_{n'} | S_T, M_T \rangle \langle S_T, M_T | \frac{1}{2}, m; \phi_n \rangle \right|^2.
\end{aligned} \tag{6}$$

The eigenstates of the total spin, $|S_T, M_T\rangle$, can be expressed explicitly as expansions over products of the adsorbate and electron spin states:

$$|S_T, M_T\rangle = \sum_m CG_{S_T, M_T, m} |S, M = M_T - m\rangle |\frac{1}{2}, m\rangle \tag{7}$$

where $|S, M\rangle$ states correspond to the adsorbate spin states and $|\frac{1}{2}, m\rangle$ to the tunnelling electron spin. The CG are Clebsch-Gordan coefficients. Combining (3) and (7) we can express the total spin states as expansions over products of adsorbate magnetic anisotropy states and tunnelling electron spin:

$$|j\rangle = |S_T, M_T\rangle = \sum_{n, m} A_{j, n, m} |\phi_n\rangle |1/2, m\rangle \tag{8}$$

The transition probability (7) then becomes:

$$P_{n \rightarrow n'} = \frac{1}{2} \sum_{m, m'} \left| \sum_{S_T} T_{Tip \rightarrow Sub}^{S_T} \sum_{M_T} A_{j, n, m} A_{j, n', m'}^* \right|^2. \tag{9}$$

In several cases, a DFT study revealed that $T_{Tip \rightarrow Sub}^{S_T}$ tunnelling amplitude is dominated by a single symmetry, S_T . This was found in the case of Mn

and Fe adsorbates on CuN/Cu(100)[22] as well as in the case of FePc (iron phthalocyanine) on CuO/Cu(110)[34]. It can be simply interpreted as the tunnelling through the adsorbate being dominated by a single orbital in the small energy range scanned in magnetic IETS. In that case, the probability (9) further simplifies into:

$$P_{n \rightarrow n'} = \frac{1}{2} |T_{Tip \rightarrow Sub}^{S_T}|^2 \sum_{m, m'} \left| \sum_{M_T} A_{j, n, m} A_{j, n', m'}^* \right|^2. \quad (10)$$

This result, used in Ref. [22], is very simple, the electronic part of the tunnelling (the $T_{Tip \rightarrow Sub}^{S_T}$ amplitude) is factored out and the probabilities for the different channels are simply proportional to spin-coupling coefficients corresponding either to the magnetic anisotropy or to the coupling between electron and adsorbate spins (the coefficients are products of the diagonalization expansion coefficients in Eq. (3) and Clebsch-Gordan coefficients).

The conductance dI/dV as a function of the STM bias, V , can then be written as:

$$\frac{dI}{dV} = C_0 \frac{\sum_n \Theta(V - EX_n) \sum_{m, m'} \left| \sum_j A_{j, 1, m} A_{j, n, m'}^* \right|^2}{\sum_n \sum_{m, m'} \left| \sum_j A_{j, 1, m} A_{j, n, m'}^* \right|^2}. \quad (11)$$

Expression (11) corresponds to the conductance for the system being initially in the ground state $n = 1$. The sum over n extends over all the $|\phi_n\rangle$ states, including the ground state, so that the above conductance takes all contributions, elastic and inelastic, into account. EX_n is the excitation energy of the magnetic level n , corresponding to the eigenvalue difference between the final, $|\phi_n\rangle$, and initial $|\phi_1\rangle$ states. The Heavyside function, Θ , takes care of the opening of the inelastic channels at zero temperature. C_0 is the total conductance corresponding to the transmission amplitude $T_{Tip \rightarrow Sub}^{S_T}$ and is then a magnetism-independent conductance. Since we only consider a limited V range, defined by the magnetic excitation energies, C_0 can be considered as constant in the relevant V -range. C_0 is equal to the conductance of the system for biases larger than all the inelastic magnetic thresholds. Expression (11) corresponds to the case where only one S_T value actually contributes to tunnelling so that the sum over j is restricted to the corresponding M_T values. If the two S_T symmetries contribute to tunnelling, a more general expression derived from Eq. (9) has to be used.

At this point, one can stress the main characteristics of the magnetic tunnelling described in Eq.(9 and 11). It reduces to sharing the electron

flux associated to a global conductance, C_0 , independent of the magnetic anisotropy, among the various anisotropy states. The inelastic transmission probability thus does not appear as a squared matrix element of a coupling but as the result of the coupling and decoupling of the electron spin with that of the adsorbate. One can see the tunnelling through the adsorbate as a spin filter that selects a specific spin-coupling between the electron and the adsorbate (the S_T symmetry); the probability of a certain n to n' transition is obtained by projecting the initial state (adsorbate n and spin of the electron m) on the spin-filter states at the beginning and by projecting the spin-filter states on the final states (adsorbate n' and spin of the electron m') at the end of tunnelling.

One can also stress that if one is only interested in the ratio between the various elastic and inelastic channels (the information yielded by magnetic IETS) and not so much by the absolute value of the tunnelling current, then only a limited input is needed to describe the process: the anisotropy constants, the spin of the adsorbate, S , and that of the tunnelling, S_T . Because of this, the above formalism can also be used to analyze experimental data in the absence of an *ab initio* study: the spectroscopic information (energy positions of the conductance steps) can be used to model the magnetic anisotropy and the step height can be used to yield the involved spin-symmetries. This strategy has been very efficiently applied by Khajetoorians et al [35] in their study of magnetic transitions in Fe atoms on an InSb(110) surface.

3.2.3. Iron phthalocyanine molecule adsorbed on CuO/Cu(110)

The case of iron phthalocyanine (FePc) molecules adsorbed on CuO/Cu(110) has been studied in detail using the strong coupling approach [34], following the experimental work of Tsukahara et al [31]. In a first step, the structure of the FePc/CuO/Cu(110) system has been studied *ab initio* using the SIESTA package [75] (only the higher symmetry β adsorption geometry has been studied). The local spin of the system is localized on the central Fe atom of the molecule. The s-electrons of Fe are transferred to the rest of the molecule and the Fe retains its $3d^6$ electronic structure. In the free FePc, the field around the Fe atom is very strong and of D_{4h} symmetry. Together with the adsorption effect, this results in a large splitting of the $3d$ manifold (see in [32, 76, 77, 78] and references therein for a discussion of the electronic structure of free FePc molecules). Real d orbitals are best adapted to discuss the D_{4h} symmetry and we keep these for the orbital notation, even in the case of the adsorbed molecule. The $d_{x^2-y^2}$ orbital is very high in energy and

unoccupied, whereas the d_{xy} is very low in energy and fully occupied. The spin structure of the adsorbed molecule then correspond to four electrons occupying the d_{xz} , d_{zy} and d_{z^2} orbitals (note that upon adsorption the d_{xz} and d_{zy} are not degenerate anymore). Following Hund's rule, the molecule is then predicted to have a spin S equal to 1, as observed experimentally. The projected density of states (PDOS) of the molecule for the various d-orbitals of Fe are shown in Fig. 8 and we can conclude that the Fe in the adsorbed molecule can be attributed the effective $d_{xy}^2 d_{y'z}^2 d_{x'z} d_{z^2}$ configuration of molecular orbitals. In a second step, the conductance between a tip and the substrate through the central Fe atom has been computed using the TRANSIESTA package for non-equilibrium transport calculations [79, 80]. In the absence of spin-orbit couplings, this package allows to compute the transmission amplitude between tip and substrate, free from the magnetic anisotropy effects, i.e. exactly the transmission amplitude that is needed as input in the sudden approximation involved in the strong coupling approach. Furthermore, this package allows to determine the eigenchannels for the transmission [81, 82]. Figure 9 presents the transmission eigenchannel with the highest transmission for two different energies: the Fermi energy and 0.2 eV above. Besides the big lobe centred around the tip, that is to be expected for a transmission eigenchannel, it exhibits a double lobe structure around the Fe atom, strongly suggestive of a d_{z^2} Fe atomic orbital perturbed by the surroundings. In addition, the same orbital shape is found for the Kohn-Sham orbital found around 0.2 eV above the Fermi level. From this, we can then conclude that tunnelling through the Fe atom dominantly involves the Fe- d_{z^2} orbital and so, that tunnelling can be described by the two effective configurations : $d_{xy}^2 d_{y'z}^2 d_{x'z}$ and $d_{xy}^2 d_{y'z}^2 d_{x'z} d_{z^2}^2$ for holes and electrons, respectively. Both configurations are doublet, hence the intermediate tunnelling symmetry (S_T in the strong coupling approach) is equal to 1/2.

We then have all the required inputs to compute the magnetic transitions induced by tunnelling electrons (if we assume the magnetic anisotropy Hamiltonian known from experiment). The corresponding results are shown in Fig. 10 which shows the relative magnitude of the various conductances, elastic and inelastic, as function of the applied magnetic field, B . Both α and β geometries are shown; it was assumed that the spin symmetries obtained ab initio in the case of the β geometry are also valid for α geometry. The strong coupling results reproduce extremely well the experimental results (Note that in Fig. 10, the step heights are normalised so that the sum of elastic and inelastic conductances is equal to 1; the excellent agreement seen in

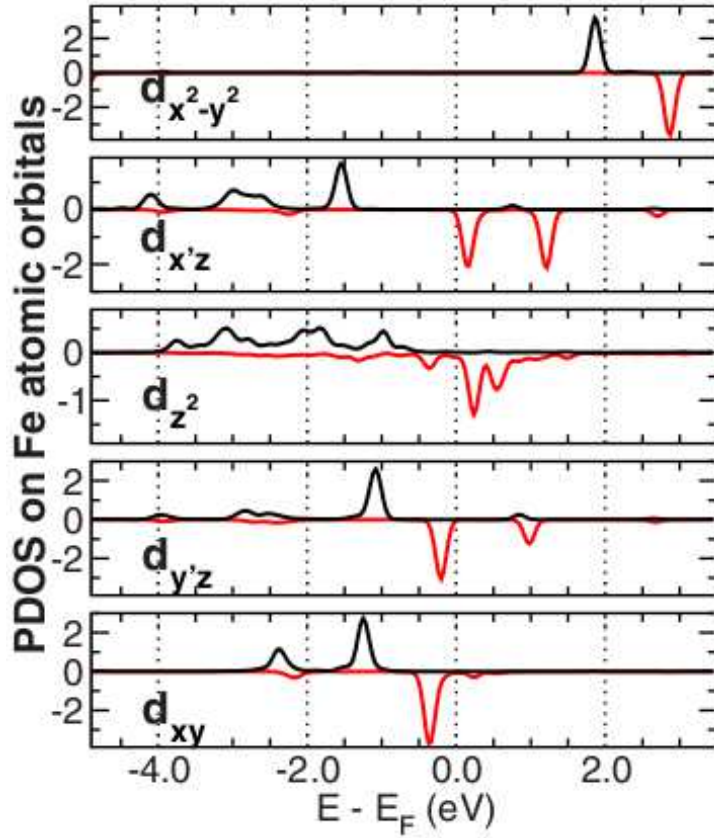


Figure 8: Projected density of states (PDOS) on the Fe d-atomic orbitals in the case of an Fe-Phthalocyanine molecule adsorbed on a CuO/Cu(100) surface. For all the curves shown here, the positive (black) corresponds to the majority spin, and the negative (red) to the minority spin. The d orbitals are classified according to the Cartesian axes that contain the N-Cu-N axis of the molecule (x, y, z), or with respect to the surface directions: x' for the $[1\bar{1}0]$ and y' for the $[001]$ directions. The z axis is the same for both reference frames. Taken from reference [34].

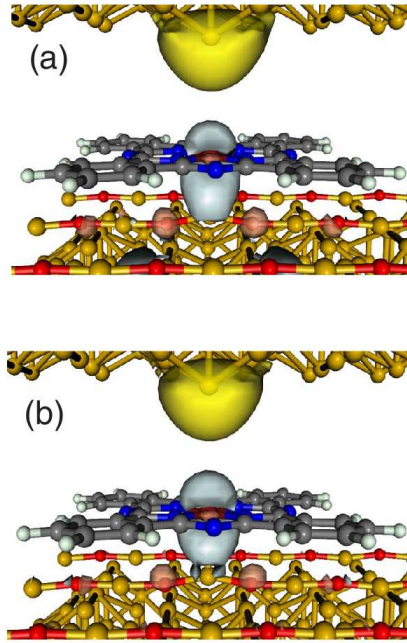


Figure 9: Transmission between a Fe-phthalocyanine molecule adsorbed on a CuO/Cu(100) surface and an STM tip modeled as an extra Cu atom on Cu(100). Transmission eigenchannel corresponding to the largest transmission amplitude for (a) $E = E_F$ where E_F is the system's Fermi energy and (b) $E = E_F + 0.2$ eV. Light gray (light pink) color corresponds to the positive (negative) imaginary part of the eigenchannel amplitude coming from the STM tip. In gold color, the positive real part. Note that the isosurfaces were chosen differently in (a) and (b) because of the large difference in transmission probability. The transmission channel exhibits a strong $a_{1g}(d_{z^2})$ character around the Fe atom. Taken from reference [34].

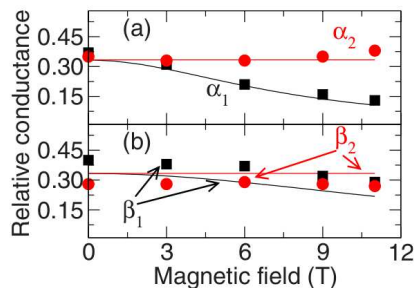


Figure 10: Magnetic IETS for an STM tip located above the Fe atom of an Fe-phthalocyanine molecule adsorbed on a CuO/Cu(100) surface. Relative inelastic step heights in the conductance as a function of the magnetic field B , for (a) α and (b) β configurations. α_1 and α_2 refer to the first and second excitation steps for the α configuration, respectively. Analogously, β_1 and β_2 refer to the first and second excitation steps for the β configuration. The experimental data points are represented with black squares for the first excitation and as red circles for the second one and are taken from the supplemental material of [31]. The theoretical results (red and black lines) are obtained in the strong coupling approach. Taken from reference [34].

Fig.10 for the inelastic conductance is thus implying an excellent agreement for the inelastic/elastic ratio). In particular, for $B = 0$, the three channels are equivalent, thus corresponding to an inelastic conductance twice larger than the elastic one. The B -variation of the relative magnitude of the various channels is also very well accounted for in the strong coupling approach. Actually this variation corresponds to the change of the magnetic structure of FePc from a structure dominated by the magnetic anisotropy imposed by the substrate at $B = 0$ to a regime dominated by the Zeeman effect at large B . The variation seen in Fig. 10 is thus the effect of the decoupling of the magnetic anisotropy by the B -field (this decoupling occurs earlier in the α geometry for which the transverse anisotropy, E , is weaker). We can see on this example the capability of magnetic IETS to emphasize the changes in the magnetic structure of an adsorbed system.

We can use the case of FePc to discuss and illustrate the selection rule in magnetic excitations. Since the transitions are induced by a spin-1/2 particle, one could say that the only possible transitions are associated with the $\Delta M = 0, \pm 1$ selection rule (only the latter two are associated with a spin-flip of the exciting electron). However, such a selection rule only applies in systems where M , the projection of the spin of the adsorbate on the quantisation axis, is a good quantum number. In the case of adsorbed FePc, at $B = 0$,

the adsorbate spin is $S = 1$, the ground and the first excited states of the system are mixtures of the $M = +1$ and $M = -1$ states, whereas the highest state is the $M = 0$ state (see details in [31]); the ΔM selection rule then does not apply. Though, one can notice that excitation from the ground state to the first excited state is a non-spin-flip transition for the electron, whereas the excitation of the second state is spin-flip. For large B fields, the Zeeman effect dominates and the various states become eigenstates of M_z . Excitation of the ground state ($M = -1$ state) then only occurs towards the $M = 0$ state (the second excited state in the B-range spanned in Fig. 10) and one can see that the magnetic excitation is indeed dominated by the excitation toward the second state in Fig. 10, as a consequence of $\Delta M = 0, \pm 1$ selection rule; this dominant process is of spin-flip character.

3.2.4. Fe adsorbates on CuN/Cu(100) surfaces

The case of Fe adsorbates on a CuN/Cu(100) substrate, which has been studied experimentally [29] and theoretically [22], is also illustrative of the characteristics of the magnetic excitation process. As discussed in section 2, the adsorbed Fe atom is associated to a local spin $S = 2$. The anisotropy brought by the substrate and an applied magnetic field splits the $S = 2$ manifold into five states. Analysis of the tunnelling process by a DFT study shows that tunnelling is associated with a $S_T = 5/2$ symmetry [22]. Figure 11 presents the relative heights of the inelastic steps in the conductance of an Fe atom on CuN/Cu(100), i.e. the relative weights of the inelastic transmission probabilities, as functions of the applied magnetic field, B . The numbers (1-3) label the excited magnetic Fe states following the order of their excitation energy. The theoretical results are seen to reproduce extremely well the experimental data and in particular their variation with the applied B field and the absence of excitation for one of the excited states. The highest level (number 4) is found to be only weakly excited in the theoretical approach and not observed experimentally, it has not been included in the figure.

The variation of the excitation probabilities with B reflects the change of magnetic structure of the system. At $B = 0$, the two lowest states correspond to the mixing of the two $|S_z| = 2$ states by the transverse magnetic anisotropy (E term in Eq. (2), see also Table 1). In this case, the strong 0-1 excitation is induced by the coupling-decoupling of the transverse anisotropy by the collision electron (initially the $S_z = \pm 2$ are coupled by E , they couple independently to the tunnelling electron spin during the collision and are coupled again together by the E anisotropy at the end of the collision) ;

such an excitation process is not associated to a spin-flip of the electron. In contrast, still at $B = 0$, the 0-2 and 0-3 transitions that involves transitions between $S_z = \pm 2$ and $S_z = \pm 1$ states are associated with a spin-flip of the tunnelling electron. At very large magnetic B fields, the system shifts to a Zeeman structure where the anisotropy effect can be neglected and where each state is associated to a given value of S_z . Then the only transitions inside the Fe $S = 2$ manifold are of spin flip type, they involve the $\Delta S_z = \pm 1$ selection rule. This aspect appears clearly in Fig. 11, where at large B , only the 0-2 transition is observed and is of spin-flip type. In this case, the adsorbate spin is initially coupled to the B field, it couples to the tunnelling electron spin during the collision and couples back to the B field at the end. On this example, one thus sees the difference between the non-spin-flip 0-1 transition at low B which implies the transient decoupling of the local spin from the substrate-induced anisotropy and the spin-flip 0-2 transition at large B which implies the transient decoupling of the local spin from the magnetic field. The gradual change of excitation probabilities seen in Fig. 11 thus corresponds to the gradual switch from a structure dominated by the magnetic anisotropy of the adsorbate to a structure dominated by the applied B field. In this way, the good agreement between theory and experiment on the inelastic intensities is a further proof of the validity of the description of the Fe magnetic structure by a local spin and the anisotropy Hamiltonian (Eq. 2)

3.2.5. Link between the various approaches

In the theoretical approaches discussed above, it could seem that the final results for inelastic transitions were different; indeed, in one case (S^2 theories), the inelastic transitions are found to be proportional to squared matrix elements of \vec{S} , the adsorbate spin, whereas in the other (strong coupling approach), everything is expressed via the total spin, \vec{S}_T , the total spin of the system (electron + adsorbate). In fact it is possible to show that the predictions of Persson's approach [73] are equivalent to those of the strong coupling approach, though without a full account of the system symmetries. In Persson's approach, the 'anisotropy-free' amplitude for tunnelling through the adsorbate is expressed as

$$T = T_0 + T_1 \vec{s} \cdot \vec{S} \quad (12)$$

with two parameters, T_0 and T_1 . We can reexpress the above tunnelling amplitude by introducing the total spin, $\vec{S}_T = \vec{S} + \vec{s}$ instead of the scalar

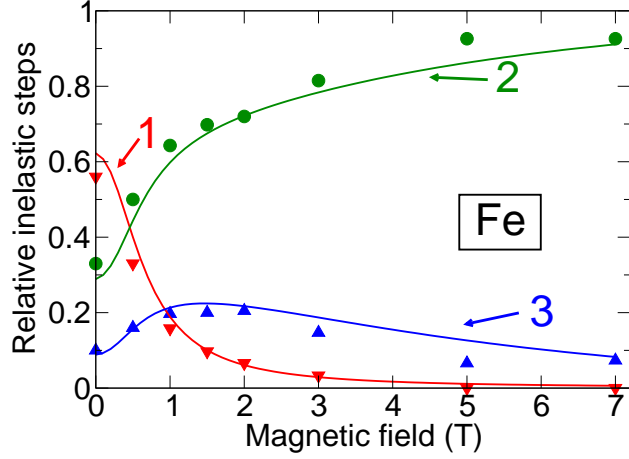


Figure 11: Relative heights of the inelastic steps in the conductance of an Fe atom on CuN/Cu(100), i.e. relative weights of the inelastic transmission probabilities, as functions of the applied magnetic field, B . Symbols: experimental data from [29] and full lines: theoretical results obtained with the strong coupling approach [22]. The numbers (1-3) label the excited magnetic Fe states following their excitation energy order. The highest state (number 4) is only very weakly excited and is not included in the figure. Taken from reference [22].

product, $(\vec{s} \cdot \vec{S})$:

$$T = T_0 + 0.5 T_1 \times (\vec{S}_T^2 - \vec{S}^2 - \vec{s}^2). \quad (13)$$

If we further introduce a closure relation on the eigenstates of \vec{S}_T^2 and S_{Tz} (quantum numbers S_T and M_T), we get:

$$\begin{aligned} T &= \sum_{M_T} |S_T = S + 1/2, M_T\rangle (T_0 + 0.5 T_1 S) \\ &\times \langle S_T = S + 1/2, M_T| + \sum_{M_T} |S_T = S - 1/2, M_T\rangle \\ &\times (T_0 - 0.5 T_1 (1 + S)) \langle S_T = S - 1/2, M_T| \end{aligned} \quad (14)$$

where $S(S + 1)$ is the eigenvalue of \vec{S}^2 . Equation (14) is exactly of the same form as Eq. (4), expressing the tunnelling amplitude as an expansion over

the different (S_T, M_T) symmetries:

$$\begin{aligned}
T &= \sum_{M_T} |S_T = S + 1/2, M_T\rangle T^{S+1/2} \langle S_T = S + 1/2, M_T| \\
&+ \sum_{M_T} |S_T = S - 1/2, M_T\rangle T^{S-1/2} \langle S_T = S - 1/2, M_T| \quad (15)
\end{aligned}$$

with the connection formulae:

$$\begin{aligned}
T^{S+1/2} &= T_0 + 0.5 T_1 S \\
T^{S-1/2} &= T_0 - 0.5 T_1 (1 + S) \quad (16)
\end{aligned}$$

Equation (16) then provides the formal link between Persson's approach [73] and the strong coupling approach [22, 34]. All factors, T_0 , T_1 , $T^{S+1/2}$ and $T^{S-1/2}$ are complex numbers and we can switch from one representation to the other. It also allows to make the link between the strong coupling approach and the extended S^2 theory ([69, 70]) using an adjusted $(u + \vec{s} \cdot \vec{S})$ transition operator. In that case, the adjusted u term only contributes to elastic tunnelling and the above equivalence thus explains the success of the original S^2 approach in describing the relative population of excited channels.

At this point, one can stress the differences for practical use of the equivalent equations (12) and (15). In the cases we studied (FePc, CoPc, Fe and Mn adsorbates ([22, 34]), tunnelling through the adsorbate is dominated by a single S_T symmetry, so that a single term has to be used in equation (15). Actually, such a situation is the one in which tunnelling is dominated by a single spin-orbital of the system. The $|T^{S_T}|^2$ term appears as a global factor in the conductance and the relative intensities in the various elastic and inelastic channels can be obtained simply from spin-coupling coefficients. In contrast, for the same situation, using Eq. (12), both terms in (12) contribute to tunnelling and only an ab initio detailed study of tunnelling can predict the relative weight of the two. As a further example, defining the S_T tunnelling channel yields the values of u in the extended S^2 formulation that would correspond to tunneling via a single S_T value: $u = (S + 1)/2$ for $S_T = S + 1/2$ and $u = -S$ for $S_T = S - 1/2$. This clearly illustrates the advantage of fully expressing the symmetry of the tunnelling process, i.e. of introducing the S_T tunnelling channels, as performed by the strong coupling approach.

3.3. Tunnelling symmetry and Single Atom Magnetisation Curve (SAMC)

As discussed above, the tunnelling symmetry (value of the total spin S_T) is extremely important for determining the magnitude of the inelastic magnetic transitions. However, it also influences other experimentally observable quantities implying polarised electrons. Indeed, measurements of the tunnelling current above an adsorbed atom with a polarised tip yields direct information about the magnetic polarisation of the adsorbate (see e.g. Refs. [24, 40, 83, 84, 85, 86, 87] and discussions therein). Among these studies, measurements of Single Atom Magnetisation Curve (SAMC) present some appealing advantages. They consist in measuring the tunnelling current with a polarised tip above the adsorbed atom as a function of an applied magnetic field [40]. For this, the tip polarisation has to survive to the applied magnetic field, i.e. to remain the same over the whole range of studied B field. If one uses a classical approach for the field dependence of the current, assuming that the tunnelling current contains a term proportionnal to the scalar product of the tip magnetisation and of the adsorbate spin, then SAMC measurements provide direct information on the polarisation of the adsorbate, its direction and the associated spin value. Actually, a SAMC presents the transition between the current for parallel and anti-parallel polarisations of the tip and adsorbates. The actual shape of the transition depends on the system temperature as well as on the magnetic anisotropy of the adsorbate. Analysis of SAMC curves imply the fit of the transition curve using a classical approach.

However, the discussion presented above about the effect of the spin symmetry (S_T symmetry of the tunnelling process) on the inelastic magnetic transitions can be transposed to the calculation of SAMC. Indeed, if we know the degree of polarisation of the tip (e.g. the fraction of electrons with up and down spins), the strong coupling approach can yield the tunnelling current as a function of the applied B field. Figure 12 presents the SAMC for a single Mn atom on a CuN/Cu(100) surface, computed using the strong coupling modelling used for the treatment of the magnetic excitation in this system [22]. The calculation of the current dependence on the B field is thus fully quantal. The tip is assumed to be fully polarised parallel to the direction of the B field, the junction bias is assumed to be larger than all the inelastic magnetic thresholds and the surface temperature is equal to 0.5 K.

Figure 12 presents the results of the strong coupling calculations for the two possible values of the tunnelling spin symmetry, $S_T = 2$ and 3 (the actual value for the Mn/CuN/Cu system is $S_T=3$, see Ref. [22]). The two

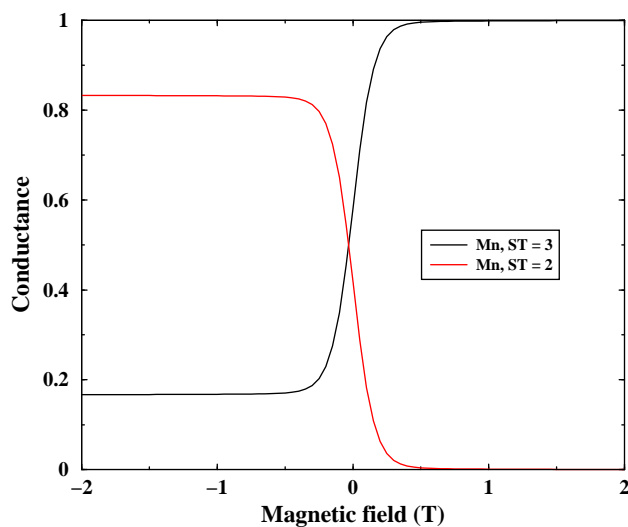


Figure 12: Single Atom Magnetisation Curve (SAMC) for a single Mn adsorbate on a CuN/Cu(100) surface. The current is computed in the strong coupling approach, using the earlier modelling of the Mn adsorbate anisotropy and spin value (Mn adsorbate spin $S = 2.5$) [29, 22]. The tip is assumed to be fully polarised, the junction bias is larger than all the inelastic magnetic thresholds and the surface temperature is 0.5 K. The SAMC is computed for the two possible values of the spin symmetry of the tunnelling process: $S_T = 2$ and 3.

SAMC appear to be very different, exhibiting opposite behaviours when the applied B field is varied. This illustrates the effectiveness of the S_T symmetry in the tunnelling process. Incident electrons with spin up and down are differently favored in the two S_T symmetries, leading to the reversal of the SAMC shape. It shows that the spin dependence of the electron transmission through a magnetic adsorbate is more complex than a mere discussion in terms of majority or minority spins, the details of the spin coupling between tunnelling electron and adsorbate have actually to be considered. Finally this also shows that the key parameter for describing the strength of magnetic inelastic transitions, the S_T symmetry, could be extracted from a spin-polarised SAMC, which does not resolve the various inelastic transitions.

3.4. Comparison with vibrational IETS: enhanced efficiency in magnetic IETS

Magnetic IETS experiments, as well as the strong coupling approach results, showed that magnetic transitions are extremely easily induced by tunnelling electrons. In several cases, inelastic tunnelling was found to dominate over elastic tunnelling, a feature at variance with vibrational IETS, where inelastic tunnelling represents at most a few per cent of elastic tunnelling [9, 17, 11, 88]. This feature can be understood in the framework of the strong coupling approach. Indeed, as seen in Eq. (10), the relative populations of the final states depends on the relative value of the $A_{j,n',m'}^*$ coefficients, i.e. on the relative weights of the final states in the intermediate j state. As discussed above, the active S_T symmetry (the j state) acts as a filter for the tunnelling and the relative weights of the final states depend on their weight in the intermediate state, i.e. in the tunnelling S_T symmetry. In this way, the process obeys spin selection rules and allow conductance cases dominated by inelastic channels.

Actually, the process as formulated in the strong coupling approach bears strong resemblances with other processes involving an angular momentum exchange in atomic, molecular or surface science. As a first example, the resonant rotational excitation of H_2 molecules by low energy electron impact has been formulated many years ago by Abram et Herzenberg [89] in a way very close to the magnetic IETS strong coupling approach. In low energy electron collisions on molecules, scattering is strongly influenced by a few resonances corresponding to the transient capture of the collisional electron by the target molecule. These are known to dominate the vibrational excitation process at low energy [90]. The resonances are also associated with a well defined molecular symmetry, i.e. with a projection of the electron angular

momentum on the intermolecular axis; very often they almost correspond to a single angular momentum in the molecular frame, $p\sigma$ wave in the case of low energy electrons colliding on an H_2 molecule discussed in Ref. [89]. The dominance of a single angular momentum in resonant scattering parallels the dominance of a single S_T total spin in the strong coupling description of magnetic IETS. In the resonant scattering process, the incident electron then brings a well defined angular momentum which couples to the molecule angular momenta; at the end of the collision, the resonance decays by emitting an electron with a well-defined angular momentum. This coupling/decoupling sequence between the electron and molecule angular momenta leads to an efficient angular momentum transfer between the collision partners. This process can be easily expressed in the sudden approximation since the rotational motion of the molecule is much slower than the electron collision, even resonant. This sudden approximation approach for rotational excitation has been much used in the field of electron-molecule collisions and the momentum exchange process outlined above was found to account very often for the observed excitation. This process also exists in the case of adsorbed molecules and lead to an efficient excitation of the frustrated rotational motion as discussed in [91, 92]. The above examples concern rotational excitation, i.e. the transfer of orbital angular momentum. However, a similar process for spin angular momentum exchange (like in magnetic IETS) has also been invoked in the case of excitation of forbidden transitions in electron-molecule transitions, both in gas phase collisions [93] and in the case of scattering on surfaces [94, 95]. Finally, one can also mention an experimental study of transitions between spin-orbit components in low energy electron collisions on NO molecules by M.Allan [96, 97]. The ground state of NO is a $^2\Pi$ electronic state which splits into two spin-orbit components: $^2\Pi_{1/2}$ and $^2\Pi_{3/2}$. At low energy, a $^3\Sigma$ resonance dominates e-NO scattering. Resonant scattering in the $^3\Sigma$ symmetry thus corresponds to a decoupling /recoupling sequence between the molecular spin and the collisional electron spin. It closely parallels the magnetic excitation process as viewed in the strong coupling approach and as a result, the $^3\Sigma$ resonant scattering is inducing strong inelastic transitions between the two spin-orbit components of the NO ground state [96, 97].

The angular momentum exchange process with a collisional electron thus seems to be of common occurrence in free molecule and surface problems and to be always of high efficiency. One can stress that the formulation used in the strong coupling approach of the magnetic IETS closely parallels the treat-

ment of the rotational excitation in electron-molecule collisions in [89]; in both cases, it is based on a sudden approximation associated to the explicit account of the angular momentum symmetry of the intermediate state and this allows to obtain the relative elastic and inelastic populations as ratios of spin coupling coefficients. In a way, it can be described as a recoil phenomenon; in the Abram and Herzenberg case, the electron in the initial and final states is associated with a well-defined angular momentum and via angular momentum conservation, scattering has to be associated to an 'angular recoil' of the molecule i.e. to rotational excitation. One can then wonder about the possibility of a similar process for vibrational excitation, i.e. for the exchange of linear momentum. In that case a recoil momentum transfer exists. Let us consider an electron scattered by a free molecule, the direction of the velocity of the electron changes in the scattering and thus the electron transfers some linear momentum to the molecule. This linear momentum recoil is the equivalent of the process discussed above for angular momentum recoil. However, due to the very large mass ratio between electrons and nuclei, the energy that can be actually transferred by a low energy electron is very weak and cannot excite vibrational motion. The situation is completely different for angular momentum exchange; due to quantization, electron and molecule angular momenta are of the same order of magnitude, allowing efficient exchange processes. Vibrational excitation then invokes usually another excitation process: resonant vibrational excitation [90, 98, 99, 100]; in that case, the long lifetime of the resonance allows a significant energy transfer between electron and nuclei, in a way during the resonance lifetime many electron-molecule interactions can occur. We can then conclude that the very efficient mechanism at play in magnetic excitations, also exists for vibrational excitations but that it is not efficient.

3.5. Excitation of magnetic adsorbates by polarized electrons, spin-transfer torque

The works described above show that the probability of magnetic excitation of an individual adsorbate by a tunnelling electron can be very large. If the tunnelling electrons are spin-polarized, then one can expect that tunnelling electrons are able to transfer part of their polarisation to the adsorbate. Indeed, electron transmission through the adsorbate can be a spin-flip or non spin-flip process; the latter does not change the adsorbate polarisation whereas the former tends to align the adsorbate polarisation with that of the tunnelling electron, i.e. to populate some specific excited states; this

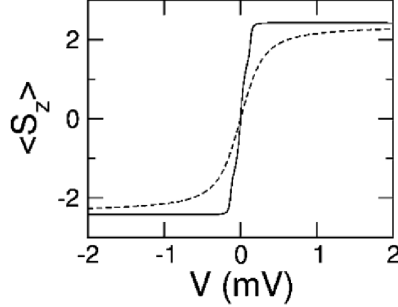


Figure 13: Model calculation of the magnetisation of a Mn adsorbate on a CuN/Cu(100) substrate. For each bias value, the steady state magnetisation of the adsorbate (mean value of $\langle S_z \rangle$) is evaluated by solving equation (17) for two temperatures: $T = 1$ K (dashed line) and $T = 0.1$ K (solid line). The tip magnetisation is parallel to the Mn easy axis. Reprinted with permission from [27]. Copyright 2010 by the American Physical Society.

spin transfer process is counterbalanced by the decay of the magnetic excited states which bring the system back to its ground state. This phenomenon is usually called 'spin-transfer torque' by reference to the capability of tunnelling electrons to rotate the adsorbate polarisation.

The spin-pumping effect has been described using a rate equation formalism [19, 27, 28]: the population of the various states of the adsorbates evolves with time due to excitation and de-excitation processes induced by the tunnelling current and by the spontaneous relaxation of the magnetic excitations. For an STM tip positioned above the adsorbate, a tip bias V and a tunneling current I , the time dependence of the population, $P_i(I, V)$, of the magnetic state, i , is given by:

$$\begin{aligned} \frac{dP_i(I, V)}{dt} = & - P_i(I, V) \left(\sum_j \Gamma_{i,j} + \sum_j F_{i,j}(I, V) \right) \\ & + \sum_j P_j(I, V) (F_{j,i}(I, V) + \Gamma_{j,i}), \end{aligned} \quad (17)$$

where $\Gamma_{i,j}$ is the partial decay rate of state i towards state j . $F_{i,j}(I, V)$ is the transition rate from state i to state j induced by the tunneling electrons.

The populations given by equation (17) very quickly reach a steady-state equilibrium, balance between spin-pumping and relaxation effects. The typ-

ical time for reaching this steady state is given by the order of magnitude of the relaxation time; as discussed in the next section, it is in the sub-ns range for the Mn/CuN/Cu(100) system going down to the fs range for magnetic atoms adsorbed directly on a metal. This is much faster than the typical time scale of an STM experiment which can then be described by the steady-state equilibrium (note, however, the existence of ultrafast STM experiments which can study magnetism dynamics in real time [38]). The first theoretical study for individual adsorbates using equation (17) was reported by Delgado et al [27, 101] on a model case; then it was further applied to the case of Mn on CuN/Cu(100) in connection with an experimental study of spin relaxation times via saturation effects [19, 28]. The spin torque effect can be very effective. Figure 13 from [27] presents the steady-state magnetisation of a Mn adsorbate (spin $S = 5/2$) as a function of the applied tip bias. It was computed using a set of parameters describing pumping and relaxation for a perfectly polarized tip. It appears that the magnetisation of the adsorbate can be easily reversed by the tunnelling current, i.e. by purely electrical means, yielding a control of the adsorbate magnetisation. In the case shown in Fig. 13 with a perfectly polarized tip, the saturation polarization at 'large' bias is almost complete. This complete switch of the adsorbate magnetisation is associated with a significant change of the adsorbate conductance, which can then yield the experimental signature of the pumping effect.

The possibility to generate a steady state population of excited states in an adsorbate allows some control on the adsorbate by electrical currents. This phenomenon has been used by Loth et al [19] to determine the relaxation times in the case of Mn adsorbates on CuN/Cu(100) (section 2). The idea is that a significant current creates a steady state population of excited states that modifies the adsorbate conductance, a careful modelling via equation (17) then allows the determination of the $\Gamma_{i,j}$ relaxation times [19]. The steady-state population of the Mn states have been modelled in Ref. [28] using ab initio computed rates for equation (17). Figure 14 presents the population of the six states of Mn (0 is the ground state and 5 the highest excited state, polarised almost anti-parallel to the ground state) as a function of the tip bias for conditions typical of experiment [19] (a partially polarised tip, magnetic field of 3 T). Consistently with Fig. 14, there exists a significant population of excited states induced by the tunnelling current that is asymmetric with respect to the tip bias. Note that for the considered currents (conductance of $2.0 \cdot 10^{-6}$ S), the population of magnetic states is drastically

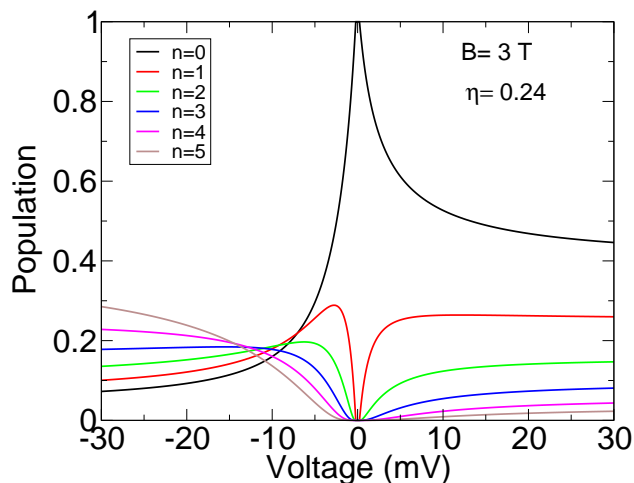


Figure 14: Population of the six magnetic states in the Mn/CuN/Cu(100) system as a function of the tip bias. The magnetic field is along the x-axis and equal to 3T. The tip polarisation, η , is equal to 0.24. The conductance at zero bias is equal to $2 \cdot 10^{-6}$ S. Taken from reference [28].

changed by the electron pumping effect, excited state populations dominating over the ground state one at large bias. This leads to drastic changes in the polarized electron conductance of the adsorbate that have been observed experimentally and theoretically [19, 28, 101]. Figure 15 presents the conductance of an individual Mn adsorbate on CuN/Cu(100) as a function of the junction bias for several values of the conductance at zero bias (this corresponds to different tip-adsorbate distances as well as to different currents flowing through the adsorbate). In this system, the magnetic thresholds are responsible for the structure at very small bias below 1 meV, whereas the variation of the conductance as the bias is further increased is due to the increase of excited state populations (see Figure 15). This variation is a direct consequence of the balance between current-dependent excitation and deexcitation induced by the electrons and current-independent spontaneous relaxation of the magnetic excitation. The use of polarized electrons allows to reveal the existence of a steady state population of excited polarized states, i.e. of the spin-transfer torque effect discussed above.

In the case of non-polarized tunnelling electrons, a large population of excited state is also generated, however symmetrically for positive and negative biases (see e.g. in [27, 28, 69]). In addition, in this case, the adsorbate conductance for large biases, far above the inelastic magnetic thresholds, is

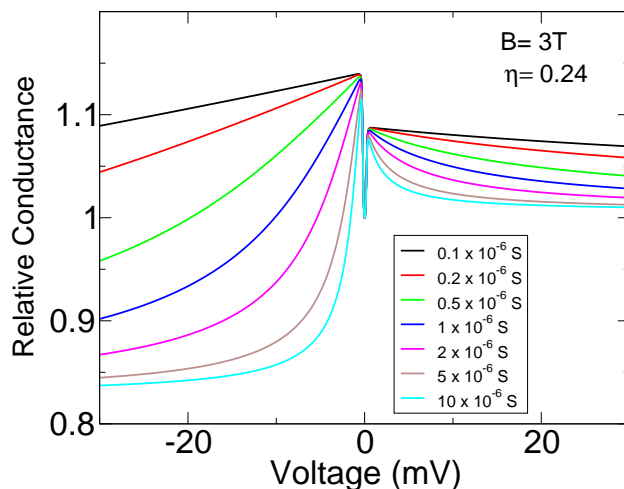


Figure 15: Relative conductance of the Mn/CuN/Cu(100) system as a function the tip bias. The tip polarization is $\eta = 0.24$ and the B field, equal to 3T, is along the x-axis. The finite population of the excited states is taken into account. The various curves correspond to various absolute conductances at zero bias ($0.1, 0.2, 0.5, 1., 2., 5.$ and $10. \cdot 10^{-6}$ S). In the figure, the conductance is plotted in relative value, with the conductance for zero bias set to 1. Taken from reference [28].

independent of the existence of a significant excited state population, as discussed theoretically and observed experimentally [19, 28, 69]. This feature can be linked with the qualitative view of the excitation process as a sharing among the possible final states[28] and is at variance with the large variations of conductance observed in the polarized electron case (see Fig. 15)).

3.6. Evaluation of magnetic state lifetimes: decay via electron-hole pair excitation

All the experimental results and theoretical studies discussed above point at the extreme efficiency of a tunnelling electron in inducing magnetic transitions in a local spin carried by an adsorbate. Actually, as is clearly seen in the strong coupling approach, the tunnelling character of the electron is not essential, in fact any electron colliding with a magnetic atom can be very efficient in inducing magnetic transitions. As a consequence, there should exist a very efficient quenching mechanism for an excited local spin on a surface: electrons coming from the substrate continuously hit the adsorbate and are scattered back into the substrate; these electrons can a priori be very efficient in inducing magnetic transitions and thus lead to an efficient quenching mech-

anism via electron-hole pair creation (an electron from the substrate with an energy lower than Fermi energy is scattered super-elastically from the excited adsorbate and goes back into the substrate with an energy above Fermi energy). This mechanism has been invoked for the interpretation of the lifetime measurements in the case of local spins on individual adsorbates [19, 38].

An extension of the strong coupling approach has been presented for the treatment of magnetic state decay via electron-hole pair creation [28]. It directly elaborates on the treatment outlined in section (3.2.2) for magnetic excitation. It makes use of the same anisotropy Hamiltonian (2) and of its eigenstates ϕ_n associated to the E_n eigenenergies. The decay rate, $\Gamma_{Tot,i}$, of an excited state, $|\phi_i\rangle$, with energy E_i , is the inverse of its lifetime τ_i and it can then be written using matrix elements of the T transition matrix (we assume the energy variation of the T matrix to be small on the energy scale of the $i \rightarrow f$ transition and we assume a vanishing temperature of the substrate) [102],

$$\begin{aligned} \frac{1}{\tau_i} &= \Gamma_{Tot,i} = \sum_f \Gamma_{i,f} = \sum_f \frac{2\pi\delta\Omega_f}{\hbar} \\ &\times \sum_{\substack{k_i, k_f \\ m_i, m_f}} \left| \langle k_f, m_f, \phi_f | \hat{T} | k_i, m_i, \phi_i \rangle \right|^2 \\ &\times \delta(\varepsilon_i - \varepsilon_f) \delta(\varepsilon_i - E_F), \end{aligned} \quad (18)$$

where $|\phi_f\rangle$ are the final states of the decay, associated to an energy transfer of $\delta\Omega_f = E_i - E_f$, and the total energy is $E_T = E_i + \varepsilon_i = E_f + \varepsilon_f$. The initial and final states of the substrate electrons are noted by their wave numbers, k_i and k_f , and by their initial and final spin projections on the quantization axis, m_i and m_f . Each term, $\Gamma_{i,f}$, in the sum over f is the partial decay rate of the initial state to a peculiar final state. The transition T-matrix can be expressed using the sudden approximation using the T-matrix defined in the absence of magnetic anisotropy (in the absence of spin-orbit coupling). Similarly to the excitation case (see section 3.2.2), the latter is then expressed as a sum over several terms corresponding to the different tunnelling symmetries, i.e. to different S_T and M_T to yield:

$$\begin{aligned} \frac{1}{\tau_i} &= \sum_f \frac{2\pi \delta\Omega_f}{\hbar} \sum_{\substack{k_i, k_f \\ m_i, m_f}} \delta(\varepsilon_i - \varepsilon_f) \delta(\varepsilon_i - E_F) \\ &\times \left| \sum_{S_T} \langle k_f | T^{S_T} | k_i \rangle \sum_{M_T} \langle m_f, \phi_f | S_T, M_T \rangle \langle S_T, M_T | m_i, \phi_i \rangle \right|^2. \end{aligned} \quad (19)$$

In the above, all the possible values of the total spin, S_T , are included. If we assume that only one spin symmetry is contributing effectively to the magnetic quenching, the expression can be further simplified to yield [28]:

$$\frac{1}{\tau_i} = \sum_f \Gamma_{i,f} = \sum_f \frac{\delta\Omega_f}{\hbar} (2\pi)^2 T^{S_T}(E_F) P_{Spin}(S_T, i \rightarrow f). \quad (20)$$

A simple expression similar to that found for excitation (equation (10)) is then recovered. In the case where the two S_T symmetries contribute to the quenching, one can make a statistical approximation justified by the summation over many substrate states and still use an expression similar to (20):

$$\frac{1}{\tau_i} = \sum_f \Gamma_{i,f} = \sum_f \frac{\delta\Omega_f}{\hbar} (2\pi)^2 T(E_F) P_{Spin}(i \rightarrow f). \quad (21)$$

the term $T(E_F)$ then corresponds to the total (all S_T symmetries) flux of substrate electrons, and is given by:

$$T(E_F) = (2\pi)^2 \sum_{k_i, k_f} |\langle k_i | T | k_f \rangle|^2 \delta(\varepsilon_i - \varepsilon_f) \delta(\varepsilon_i - E_F), \quad (22)$$

which can be easily implemented in DFT [28]. The probability $P_{Spin}(i \rightarrow f)$ is defined as an average over the two S_T values.

The physical meaning of equations (20) and (21) is transparent, it can be interpreted as the product of the number of electrons hitting the adsorbate per second in the appropriate energy interval by a spin-transition probability. The spin-transition probability is expected to be significant and the flux factor, $T(E_F)$, to depend on the system under investigation. In particular,

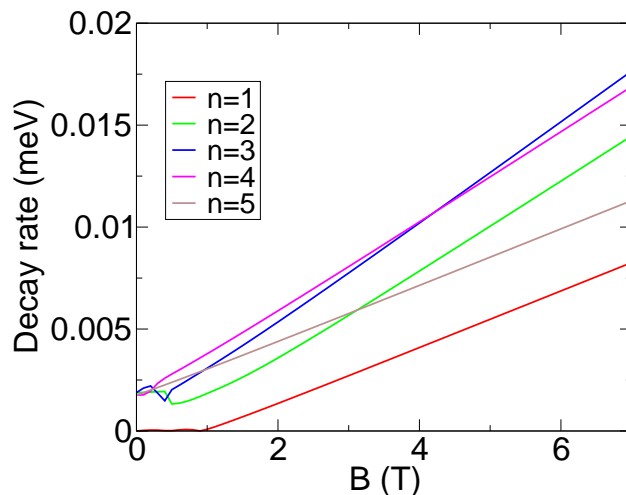


Figure 16: Decay rate (in meV) of the five excited magnetic states of a Mn atom on CuN/Cu(100) as a function of an external magnetic field B . Taken from reference [28].

one can expect the presence of an insulating ultra-thin layer between the adsorbate and the substrate to reduce the flux factor.

The flux factor bears strong resemblances with the tunnelling term in the excitation formalism. Actually, it has been shown [28] that it can be calculated from first principles using an approach very similar to the one used in the TRANSIESTA code to compute tunnelling fluxes. The idea is to introduce a single reservoir (the substrate) instead of two (the substrate and the tip) and to compute the flux from the reservoir into the reservoir via the magnetic atom; the latter is defined by a set of atomic orbitals.

This approach has been used in the case of Mn adsorbates on CuN/Cu(100) studied experimentally by Loth et al [19]. The corresponding results for the decay rate as a function of the applied B field are shown in Fig. 16. The spin, S , of the Mn adsorbate is $5/2$, so that there are five excited states. As seen in Fig. 17, the decay rate of the lowest lying state is very small at small B; this is a direct consequence of the adsorbed Mn magnetic structure and not so much a sign of stability of the state: the lowest state has a very small excitation energy at low B, so that its decay rate is very small (see Eq. (20)). Besides this energy effect, typically, the decay rates are in the range of 2 to 20 μeV , corresponding to lifetimes of the order of 0.3-0.03 ns. One can notice that the decay rates increase with the applied magnetic field, almost linearly at large B. This is also an effect of the de-excitation energy;

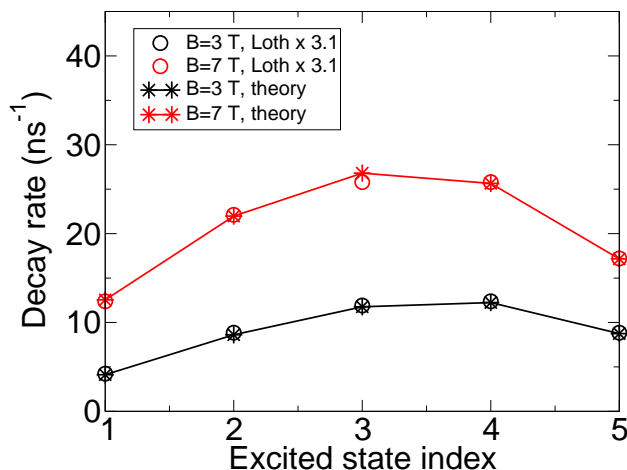


Figure 17: Comparison between the theoretical decay rate (stars) of the five excited magnetic states in the Mn/CuN/Cu(100) system with the experimental results of Loth et al [19] (open circles). The black symbols correspond to an applied B-field of 7T and the red symbols to 3T (the B-field is along the x-axis). The lines are only guides for the eye. For the sake of comparison, the experimental results of Loth et al have been multiplied by a global factor equal to 3.1. Taken from reference [28].

in the Zeeman limit at large B, the energy difference between the states vary linearly with B and so do the decay rates.

These magnetic lifetimes are rather short, so that it seems likely that the electron-hole pair creation process will dominate the excited state decay over other processes, involving e.g. atomic motions [37]. Figure 17 presents a comparison between the strong coupling results and the experimental results [19, 28]. The relative values of the decay rates (ratio between excited states, dependence on B) is well accounted for, but the theoretical results are a factor 3.1 larger than the experimental data. The origin of this discrepancy is not clear.

The theoretical estimate for the decay rate (expression (21)) can be used to discuss the possible variations of the magnetic state lifetime, i.e. of the relaxation time of a local magnetic moment on an adsorbate. Besides the excitation energy term, already discussed, two effects could lead to very different lifetimes, short or long. First, the flux factor can be very different on different substrates; for example, a 'thick' layer of an insulator could effectively decouple the surface from the underlying metallic substrate and significantly decrease the flux at the adsorbate leading to very long-lived

states. Similar effects have been invoked to explain long-lived states (non-magnetic, delocalised or localised) at metal surfaces in the presence of insulating layers [103, 104, 105, 106, 107]. Another variation could come from the spin-probability factor. Certain spin structures could be designed such that transitions induced by electrons between an excited state and the ground state are forbidden or quasi-forbidden; this can happen e.g. in the case of a local spin with a large anisotropy (large negative D in Hamiltonian (2)) at finite B field. In this case, the two lowest lying states are quasi-Zeeman states (almost eigenstates of M_z), which do not fulfill the $\Delta M = 0, \pm 1$ selection rule. This structure has been suggested in Ref. [29, 108] as a possible model for bistable systems; the long lifetimes found by [38] in the case of Fe and Cu adsorbed on CuN/Cu(100) also pertains to this class of systems.

In this context, one can mention a series of theoretical studies devoted to individual 3d magnetic atoms adsorbed directly on a metal substrate [24, 109, 110, 111]. In that case, the coupling between adsorbate and substrate is much stronger than in the case discussed above that involved a partly insulating layer between adsorbate and metal. This leads to a strong hybridization between the atom and the metal and ultimately to much reduced lifetimes for the magnetic excitations. Theoretically, these systems were treated using an itinerant magnetism kind of approach instead of the local spin concept discussed above. The susceptibility of the adsorbate/substrate system, response to an applied oscillating transverse magnetic field, was computed taking into account the effective interaction between electrons. The susceptibility as a function of the excitation frequency displays peaks at the allowed excitation energies, the width of which corresponds to the excited state lifetimes. The decay of the excited magnetic states is again due to electron-hole pair creation, called Stoner excitations in this context. In the case of Fe adsorbates on Cu(111), also studied experimentally by magnetic IETS [24], the theoretical lifetime of the excited magnetic state was found to be very short, typically in the 500 fs range, in excellent agreement with the measured linewidth. The level width is seen to vary almost linearly with the applied magnetic field, basically following the variation of the excitation energy of the state (see above a discussion of this effect for local spins). Actually, it appears that the level width of the excited magnetic state is almost equal to the excitation energy of the state, confirming its highly unstable character and explaining why the excited state is only observed as a very broad structure and not as a sharp step in the conductance in a magnetic IETS experiment.

3.7. Chains of magnetic atoms and spin wave excitation

All the theoretical studies discussed above considered the case of a single magnetic adsorbate on a surface, carrying a local spin. In connection with experiments on chains of magnetic adsorbates, several theoretical studies addressed the problem of chain excitation and its links with spin-wave excitation in an infinite 1D-spin chain. The first study considered the case of short linear chains of Mn adsorbates coupled by magnetic exchange [71], following an experimental study on the same system [43]. It considered the following Hamiltonian to describe the structure of the chain:

$$\begin{aligned} \hat{H} = & \sum_i D \hat{S}_{i,z}^2 \\ & + E(\hat{S}_{i,x}^2 - \hat{S}_{i,y}^2) + g_i \mu_B \vec{S}_i \cdot \vec{B} + \sum_{i,j} J_{i,j} \vec{S}_i \cdot \vec{S}_j \end{aligned} \quad (23)$$

The sums over i and j run over the Mn sites in the chain. It thus considers a set of local spins, \vec{S}_i , each interacting with the surroundings via an anisotropy Hamiltonian and coupled together by Heisenberg exchange couplings (in the present Mn case the coupling between first neighbours is anti-ferromagnetic). Using the perturbation approach to justify the S^2 formula (see section 3.2.1), the conductance for a tip positioned above a given atom in the Mn chain is obtained. These results are shown in Fig. 18 for a number of Mn atoms between 1 and 4 (taken from [71]). As the main feature, this study confirms very well the odd-even alternance of the conductance that has been observed experimentally [43]. It appears as a direct consequence of the spin structure of the chain: in a finite chain, the ground state corresponds to a total spin equal to zero ($5/2$) for the even (odd) numbers of atoms, leading to a very different energy spectrum of excited states. Another interesting feature appears on the results for a chain of three atoms: the conductance is different for the tip positioned above the central atom and above the end atom; it concerns both the number of steps in the conductance and their heights. This is linked with the symmetry of the problem: a central excitation is symmetric, whereas exciting at the end of the chain can be symmetric or antisymmetric. However, in the experimental paper [43], it is mentioned that the conductance does not vary along the chain. The origin of this discrepancy is not clear.

The strong coupling approach has also been applied to the problem of excitation of chains of magnetic atoms with an STM tip [44]. A model system was considered, made of a spin-1/2 chain of atoms, with first neigh-

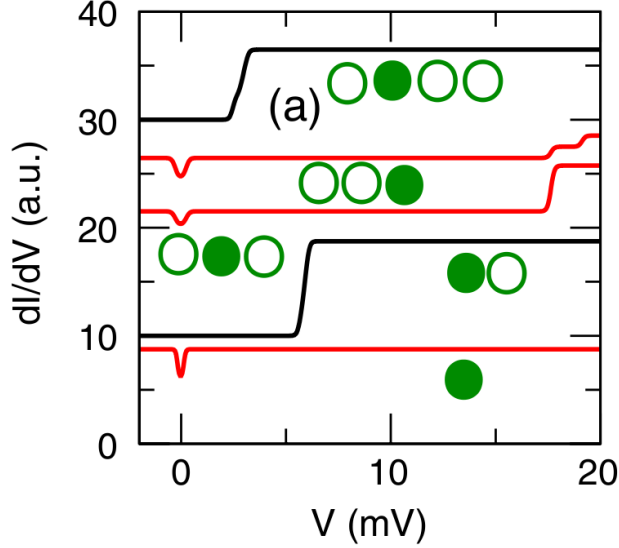


Figure 18: dI/dV for $B = 0$, $k_B T = 0.6$ K for chains of N Mn atoms, $N = 1, 2, 3, 4$. Solid circles represent the atom underneath the tip. Reprinted with permission from [71]. Copyright 2009 by the American Physical Society.

bours coupled by an Heisenberg exchange interaction (ferromagnetic or anti-ferromagnetic). The formulation closely follows the one outlined above in section 3.2.2, except that the anisotropy Hamiltonian describing the interaction between the local spin and its environment is replaced by a Heisenberg chain interaction ($\sum_i J \vec{S}_i \cdot \vec{S}_{i+1}$) representing the interaction of each local spin with its neighbours. It is assumed that tunnelling is very fast so that the Heisenberg interaction can be neglected during tunnelling and a sudden approximation can be used; it is also assumed that this fast tunnelling only concerns one atom at a time, thus leading to the definition of the total spin S_T channels ($S_T = S \pm 1/2$, where S is the local spin of one site of the chain). This model then describes a chain of individual adsorbates, only coupled via magnetic exchange.

The conductance of this system has been studied for various lengths of the chains, with up to 18 atoms. The aim was to look for general trends in the chain excitation, as well as to the conductance behaviour when the number of atoms in the chain goes to infinity, i.e. when spin wave modes can be defined. Actually, it appears that finite chains with a ring boundary condition (a

Heisenberg chain of N atoms with a periodic boundary condition: $S_{N+1} = S_1$) can be considered as approximations of the infinite system thus allowing the discussion of the characteristics of spin wave excitation by tunnelling electrons in 1D-Heisenberg chains. In other words, the spin wave modes confined in a finite-size object, a ring, become quantized and they constitute a sub-set of the excited states in a finite size chain (note that the number of states in a chain of N atoms is equal to 2^N and becomes extremely large when N is large).

In the ferromagnetic case, a finite-size ring of atoms can be considered as a piece of the infinite system. In the ground state, all local spins are aligned to form a state of maximum spin ($S_{Tot} = N/2$, in the present case with spin-1/2 sites). Excitation by a tunnelling electron only populates the states with $S_{Tot} = N/2 - 1$, which correspond to the spin wave mode or 'magnon'. So, only very specific states among all the available excited magnetic states in the chain are actually excited by a tunnelling electron. The spin wave excitation is very efficient, similarly to the case of a single adsorbate on the surface. From the analysis of the excited states of a ring that are populated by tunneling electrons, it is possible to extract the k -distribution of the excited waves (k is the spin wave momentum). The k -spectrum of the excited spin waves is white (all k -values are populated with equal probability) which allows to derive simply the energy-spectrum of the excited spin-waves and thus to fully characterize the spin-wave excitation by a tunnelling electron [44]. The equi-probability of all k -states is a direct consequence of the nature of the excitation process: the flip of a local spin in an infinite ferromagnetic chain, i.e. a δ -like excitation.

The anti-ferromagnetic case is quite different. First, a finite size ring of atoms is only an approximation of the infinite system due to strong correlations between distant spins (see discussions in e.g. [112, 113, 114, 44] and in text books [30, 115]), so that one has to look for the convergence of the conductance when N goes to infinity. The ground state of a chain with an even number of atoms corresponds to a total spin S_{Tot} equal to zero and the spin wave mode corresponds to a set of $S_{Tot} = 1$ states. Figure 19 shows the conductance for a series of rings of different lengths, $N = 10 - 18$. It appears that a very large number of magnetic states in the ring are excited by a tunnelling electron (there is a very large number of steps in the conductance function of bias). All these excited state contributions build a complex step function; however, if the number N of atoms in the ring is changed, the step positions and heights change, but the continuous curve that would be

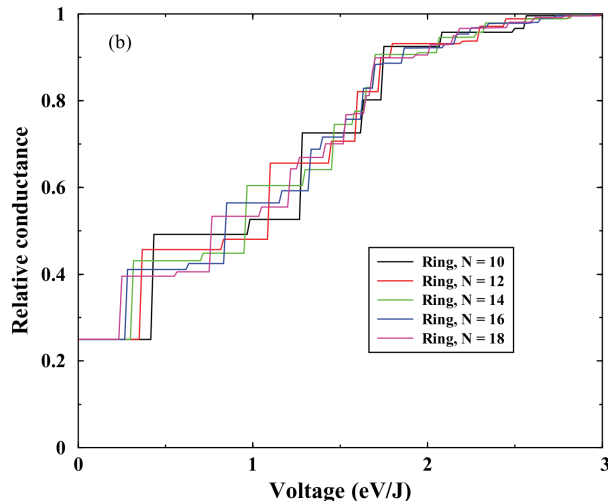


Figure 19: Relative conductance of a ring of antiferromagnetic atoms as a function of the tip bias (in units of J). The conductance has been normalized to one above the inelastic magnetic thresholds. Five different numbers of magnetic atoms are presented: $N = 10$ (black curve), $N = 12$ (red curve), $N = 14$ (green curve), $N = 16$ (blue curve), and $N = 18$ (magenta curve). Taken from reference [44].

obtained by smoothing out the steps does not. Consequently, the conductance functions with many steps can be considered as approximations by step functions of a continuous curve that corresponds to the conductance of an infinite chain, i.e. to the excitation of spin waves. It also appears that many more states are excited, beyond the 'usual' spin wave mode, in particular many states excited by tunnelling electrons belong to the continuum of two-spinon states [116, 117] (two-spinons form a continuum and quantization in a finite size ring transform them into discrete states forming several 'spin-wave modes' at energies higher than the 'usual' low lying magnon mode).

Figure 20 presents the k -distribution for various numbers of atoms in the ring (see insert); it corresponds to the sum of all the excited spin wave modes. Due to the finite size of the ring, only a finite number of k -values are determined for each number N of atoms. It appears that the convergence of the k -distribution with the number of atoms in the ring is excellent, so that the distribution in Fig. 20 can be considered as the result for spin wave excitation in an infinite 1D-chain. It also appears that the distribution peaks at the outer edge of the Brillouin zone, in contrast to the ferromagnetic case where all k -values are equiprobable. This is connected with the different

qualitative views one can have of the excitation process in the ferro and anti-ferromagnetic cases. In the ground state of the ferromagnetic chain, all spins are aligned; only an incident electron with an anti-parallel spin can excite the chain and the only excitation it can induce is a spin-flip of the atom through which tunnelling occurs. As a consequence, in a ferromagnetic chain, only the spin wave mode is excited with all k -waves equally populated. The situation is different for anti-ferromagnets: due to the multiconfigurational character of the spin wavefunction, a given atom in the chain does not have a well defined spin. However, tunnelling of an electron with a given spin through an atom selects a well defined S_T spin coupling between the electron and the active site in the chain. For example, if tunnelling implies the $S_T = 0$ channel for a spin-1/2 atom, this will select in the multiconfigurational expansion of the chain ground state only the components that correspond to a spin of the adsorbate opposite to that of the tunnelling electron. The tunnelling process thus selects a part of the ground state wavefunction; basically half of the ground state wavefunction is projected out and this projection directly induces the excitation of many chain states. This correlation-mediated excitation is very broad and concerns many states. It emphasizes the correlations present in the chain ground state; in particular the two-atom period present in the chain correlation appears in the correlation-mediated excitation process and leads to a k -distribution peaked at the edge of the Brillouin zone.

This study of the excitation of Heisenberg chains has been extended to the case of frustrated ferro-magnetism in spin-1/2 chains [118]. Indeed, it has been shown that a Heisenberg chain with ferromagnetic coupling between first neighbours and anti-ferromagnetic coupling between second neighbours leads to a variety of magnetic structures when the relative magnitude of the exchange couplings is changed and when a magnetic field is applied; as said in Ref. [119], 'the ground state phase diagram ... is a zoo of exotic quantum phases' (see discussions in [120, 121, 122, 123] and references therein). Besides the fascinating properties of these structures, the theoretical activity in the field was partly prompted by experimental studies of various systems that were interpreted as frustrated 1D-spin 1/2 chains (see e.g. [124, 125, 126, 127] and references therein). Such chains supported on a surface can be excited by tunnelling electrons and Ref. [118] studied how the variety of magnetic structures in the chain is reflected in the characteristics of the chain excitation by tunnelling electrons. Surprisingly, the changes in junction conductance following changes in the chain magnetic structure was found in most cases not to be very strong. However, it was shown that the use of polarised electrons

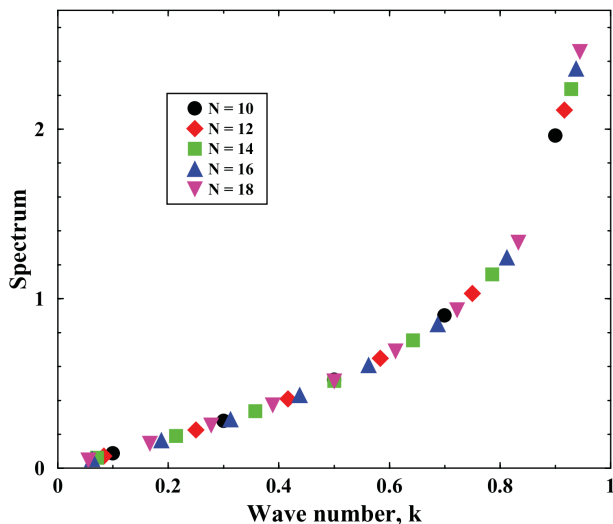


Figure 20: Spectrum summed in energy of the spin waves excited by a tunneling electron in a ring of antiferromagnetic atoms as a function of their wave number k . The wave number is expressed in units of π/a , where a is the lattice spacing. Results for different numbers of atoms in the ring are presented: see inset. Taken from reference [44].

for exciting the chain could be used to identify structural features in the chains. In addition, in such frustrated chains, helical features of the ground state, remnants of the classical spiral structure, can only be seen in correlation functions; but excitation of the chain by tunnelling electrons can reveal the underlying spiral structure. This is connected with the excitation process at play in this system which bears much resemblance with the process active in pure anti-ferromagnetic chains that was outlined above. Selection of a S_T channel for the tunnelling process, selects only a part of the correlation expansion describing the chain ground state and this correlation-mediated process leads to a broad excitation spectrum; it also uncovers some hidden properties of the correlations in the chain, such as the helical feature, that become visible in the momentum spectrum of the spin waves excited by a tunnelling electron [118].

4. Kondo effect and IETS

The above sections have reviewed the very fast developments in magnetic IETS with the STM since the first experiments [12] by Heinrich and

co-workers in 2004. As a spectroscopy, the technique has revealed the magnetic structure associated with single magnetic impurities on a non-magnetic substrate. This is deeply linked to Kondo physics. Indeed, Jun Kondo [128] showed that magnetic impurities in a non-magnetic host undergo spin-flip scattering by the host's conduction electrons leading to an increase of resistivity as the temperature is lowered below a given value. The main difference with the magnetic IETS mechanism expounded above is that the spin-flip scattering takes place at zero energy: there is no exchange of energy between the incoming and outgoing electron, contrary to the above inelastic processes.

In the present section, we are going to restrict ourselves to the link between the Kondo effect and IETS, without dwelling upon the very extensive literature associated to the Kondo effect on surface and particularly its study with the STM [129, 130, 131].

As temperature is lowered, the spin-flip scattering becomes coherent [132]. Electrons become correlated and at low temperatures the ground state of the full system reveals the spin-flip process by screening out the magnetic moment of the magnetic impurity. The ground state is a singlet. As temperature is raised, electron-hole excitations become available, and the system is not in its ground state any more. The appearance of excitations lead to decoherence of the spin scattering process and the impurity recovers its magnetic moment.

The electronic spectrum of such a Kondo system in its ground state is characteristic of strongly correlated systems. We just saw that the ground state is a singlet, and the first excitations recover the local magnetic moment of the impurity. If we take the full electronic spectrum of the system and keep the electronic structure that has information on the impurity's state, we study the projected density of states onto the impurity's orbitals also known as spectral function. Figure 21 shows a typical Kondo spectral function for the case of very large intra-impurity Coulomb repulsion. At low temperature, this spectral function shows a broad peak that is largely occupied and represents the Kondo ground state [132, 133]. At just the Fermi energy, a new peak appears that represents the first excitations of the system. The first peak under the Fermi energy is the usual resonance of a localized electronic state in front of an electronic continuum, it is sometimes called the charge fluctuation peak to emphasize its origin in the electron hybridization between impurity and substrate [132, 133]. The second peak of low-energy excitations, hence just above the Fermi energy, is the spin-fluctuation peak. This peak is sometimes called the Abrikosov-Suhl resonance or simply, the

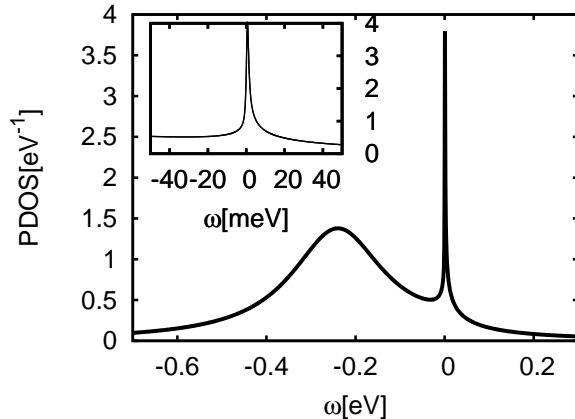


Figure 21: Projected density of states on the magnetic adsorbate electronic structure or spectral function A as a function of the electron energy ω with respect to the Fermi energy of the substrate. The impurity has a single electronic level that gives rise to the broad Lorentzian curve below the Fermi energy and the electron-electron repulsion is very large so that the doubly occupied state is far above the Fermi energy. Near the Fermi energy the sharp Kondo resonance develops. The insert presents an close view at the Fermi energy range. Taken from reference [134].

Kondo peak. The Kondo peak is a hallmark of the Kondo effect. Since it is a spectral feature of the magnetic impurity, it can be easily revealed by conductance measurements with the STM. Indeed, the STM conductance is closely related to the local density of states. When the STM tip is located at the impurity, the impurity's spectral function usually dominates the conductance, and a peak at zero bias reveals the Kondo effect.

Actual STM measurements are quite involved and the complete characterization of the Kondo peak requires several measurements. However, the Kondo peak has some unique features that makes it totally different from any other source of a zero-bias anomaly. These feaures are:

1. The temperature dependence of the width of the peak. At very low temperature the peak's width saturates to $2k_B T_K$ where T_K is the so called Kondo temperature and sets the energy scale at which Kondo physics takes place. Hence, the peak's width, γ , follows the law [135]

$$\gamma = 2k_B \sqrt{(2T_K)^2 + (\pi T)^2} \quad (24)$$

2. The peak dependence with an external magnetic field, \vec{B} . An external magnetic field induces a Zeeman splitting of the impurity's magnetic

levels, hence spin up scattering is not any longer degenerate with spin down scattering and the Kondo effect is destroyed. However, its destruction is not complete, because electrons of higher energy can interfere with opposite spin electrons if their energy difference is exactly the Zeeman splitting. Indeed, we are describing an inelastic effect and at the energy threshold of this inelastic effect the electrons can spin-flip coherently recovering a Kondo peak, but instead of being centered near the Fermi energy, the new peak is centered at the energy of the excitation. Since electrons above the Fermi energy and below (holes) can produce this inelastic effect, there are two new peaks that appear replacing the previous Kondo peak when the magnetic field is switched on. For very large fields coherence cannot be achieved and all peaks disappear, or in other words, the impurity's magnetic moment cannot be screened out at large external magnetic fields.

Both the temperature and magnetic field behaviors permit us to characterize a zero bias anomaly as due to the Kondo effect. However, experiments are further complicated by the fact that these anomalies are rarely pure peaks. Indeed, they present Fano lineshapes that are more difficult to analyze. The origin of the Fano lineshape comes from the contribution of many electronic states to the STM conductance other than the impurity's ones [136].

A further difficulty is the typical energy scale in the Kondo problem. Rarely a Kondo temperature goes above 100K. Larger temperatures typically mean that the charge fluctuation peak and the spin-fluctuation peak start overlapping and a pure Kondo effect is no longer available: in fact, charge fluctuations rapidly override spin ones, and the system is a mixed-valence one, that fluctuates between several charge states. The spectral features are very broad at the Fermi energy.

Due to the particular electronic structure of atomic and molecular substrates the Kondo temperatures are anywhere between a few Kelvin and ~ 100 K. This is in stark contrast with the initial quantum dot studies of Kondo effects where typical temperatures were in the milli-Kelvin range making it more difficult to measure. Usual low-temperature STM's are capable of measuring adsorbate Kondo peaks. But they need to be able to change their temperatures in a very controlled way within a few K to be able to probe the above temperature dependence, Eq. (24). They also need to be fitted with a magnetic field. However, due to the small Bohr magneton value

(57.9 $\mu\text{eV}/\text{Tesla}$) very large magnetic fields are mandatory to be able to discern the above splitting of the Kondo peak. At large Kondo temperatures, the splitting can be simply undetectable.

Besides these difficulties, the STM has become a successful tool to reveal coherent spin-flips in magnetic adsorbates.

4.1. *Inelastic spin-flip and Kondo effect*

As mentioned above, the impurity-substrate system in an excited state does not exhibit Kondo physics anymore. However the transition from a correlated ground state to an uncorrelated excited state is gradual. Zaránd and co-workers [137, 138] have undertaken the study of this transition. The appearance of the Kondo ground state can be seen as the screening of the magnetic impurity in such a way that the impurity behaves as a strong but conventional potential scatterer where inelastic effects are absent. Zaránd and co-workers [137, 138] have studied the energy dependence of the inelastic scattering rate as the impinging electron energy is increased. These authors take the total cross section of the electron-impurity scattering and then subtract the elastic contribution to the cross section, defining in this way the inelastic part. By virtue of the optical theorem, the total cross section is obtained from the imaginary part of the diagonal T-matrix, while the elastic part is obtained from the on-shell Golden-rule like expression using all terms from the T-matrix. They obtained the T-matrix from a numerical renormalization group calculation and use Fermi liquid identities to evaluate the absolute values of the electron cross section.

They show that most of the scattering for electron energies above the Kondo temperature, T_K , is inelastic. At energies below T_K the total cross section saturates, as well as the elastic one. The inelastic cross section presents a maximum at about T_K . As the energy decreases towards the Fermi energy (here taken as zero), the inelastic cross section diminishes with the square of the electron energy. This is expected from Fermi liquid theory, since the quasiparticle lifetime scales with the square of the electron energy close to the Fermi energy. When the electron energy increases past T_K , the inelastic cross section diminishes again, this time with $\sim 1/\ln^2(\omega/T_K)$, with ω the electron energy. This behavior is due to the dominance of spin-flip scattering at large electron energies.

This study shows how inelasticities destroy the Kondo effect, and permits to characterize the onset of inelastic spin-flip scattering as the electron energy increases.

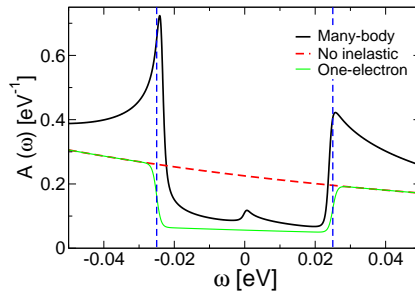


Figure 22: Projected density of states on the magnetic adsorbate electronic structure or spectral function A as a function of the electron energy ω with respect to the Fermi energy of the substrate. The vertical dashed lines show the one-electron inelastic thresholds. Taken from reference [140].

4.2. Magnetic IETS and Kondo effect

Different from the above case concerning the destruction of the Kondo ground state by inelastic processes is the study of the impurity's magnetic structure with impinging electrons. Zitko and Pruschke [139] have applied Kondo theories and described the coexistence of a Kondo peak as well as IETS steps in the STM conductance of Co atoms on CuN/Cu(100) substrates. Indeed, Kondo theories include information on incoherent spin-flip scattering leading to IETS. Moreover, one can picture the IETS process as a Kondo one at the excitation threshold because, at threshold, the elastic and inelastic spin-flips are degenerate, and hence coherent. It is then possible to obtain the same type of singular behavior as the Kondo peak, but at the IETS thresholds.

This has been the subject of study by Hurley and collaborators [49] and Korytár et al [140]. Hurley and collaborators [49] use perturbation theory to analyze the magnetic IETS of Co and Fe on CuN/Cu(100). The authors conclude that certain spike-like thresholds at the steps of the experimental IETS are due to Kondo-like peaks. Korytár et al [140] use a self-consistent approach to study the excitation of a singlet molecule to its triplet state. This type of singlet-triplet excitations have already been studied experimentally in Mn chains with an even number of atoms [43], in carbon nanotubes [50], in C_{60} molecules [51], and in cobalt complexes [52].

Korytár and collaborators [140] explicitly include an exchange interaction between two localized electrons that belong to different orbitals. This model has been used to explain the experimental behavior of copper phthalocyanine on Ag (100), showing that the Kondo system is related to a triplet-singlet

spin transition [134] as shown in the experiments by Mugarza et al [141]. The exchange interaction is then:

$$\hat{H}_I = I\vec{S}_1 \cdot \vec{S}_2. \quad (25)$$

For positive I , the impurity is a singlet and it is not subjected to the Kondo effect. As a result there is no peak at zero energy. The triplet state lies at exactly I above the singlet state in this model. However, as the electron energy increases, the triplet state becomes available under an inelastic spin-flip process. At threshold, both spin states become degenerate and spin-flips keeps its coherence giving rise to singular-like peaks. Figure 22 shows the spectral function for such a system. In the same graph, the above one-electron results for magnetic IETS is also plotted. We see that many-body effects included via the self-consistent approach substantially change the spectral function. The most noticeable feature is the new peaks that considerably change the overall shape of the spectral function. But also the excitation thresholds are perturbed. The thresholds are shifted to lower energies. This is an important effect for the determination of magnetic energies based on IETS: many-body effects can renormalize the IETS thresholds.

The strength of the threshold renormalization is found to depend on an energy scale that replaces the Kondo temperature and is called T_K^0 in Ref. [140]. Indeed, if $I = 0$, a Kondo effect appears with Kondo temperature T_K^0 . Another parameter of the strength of the threshold renormalization is I . It is interesting to study the change in the excitation energy, called ΔI , as a function of I . For large I , the threshold renormalization, ΔI , follows a $I/\ln(I/T_K^0)$ behavior, similar to the renormalization found for the shift of Kondo peaks with an external magnetic field [142, 143]. The resemblance of the present results with the ones found in the presence of magnetic fields is due to the similar physical process: in both cases, there is a magnetic excitation, in the present case due to the interaction between two localized spins, and in the magnetic-field case due to Zeeman energy splitting, and when the electron energy is large enough to open the excited channel, the ground and excited states are connected via spin flip.

The emergence of the excitation energy, I , as a new energy scale for Kondo physics in the presence of magnetic excitations, can be further revealed by studying the impurity's spectral function behavior with temperature [140]. When $I = 0$, the system displays a characteristic Kondo temperature, named T_K^0 above. At temperatures T larger than T_K^0 , the Kondo peak is very diminished. However, when $I \neq 0$, the new Kondo peaks appearing at the

excitation thresholds persists well beyond T_K^0 , showing that a new type of Kondo physics is appearing. When the temperature matches I , the Kondo peaks at the excitation thresholds coalesce and there is a unique Kondo peak that persists at higher temperatures. Hence I becomes an important energy scale when considering Kondo effects.

The physics behind this new energy scale can be understood by looking at the effect of thermal electron-hole pairs. For $I = 0$, both initial and final electrons have the same energy after scattering off the magnetic impurity. Hence, both states are subject to the decoherent effect of thermal electron-hole pairs near the Fermi energy. As a consequence, beyond T_K^0 , decoherence becomes very large and the Kondo peak vanishes. When $I \neq 0$, the initial electron is at I away from the Fermi energy, if the temperature is smaller than I , then these electrons will not be affected by the decoherence induced by thermal electron-hole pairs. As a result, the new Kondo physics is more resistant to higher temperatures.

5. Conclusions

The extraordinary extension of the STM to very low temperatures with built-in magnetic fields has permitted the development of magnetic inelastic electron tunneling spectroscopy with subatomic resolution. New measurements have revealed the low-energy scale associated with the magnetic anisotropy of adsorbates on solid surfaces. Atomic adsorbates have been explored on different metallic surfaces either with an insulating layer to decouple the adsorbate, such as MgO [12] or CuN [43, 29], or on the surface itself [36, 24]. Also, IETS proved to be extremely useful in the study and characterisation of magnetic impurities on semiconducting substrates [35]. Non-atomic adsorbates such as magnetic molecules [31, 46] and layers of magnetic molecules have also been studied revealing not only the intramolecular magnetic properties but also intermolecular interactions. All these experiments show that magnetic IETS is a full-fledged, versatile technique of extreme usefulness. Its older sibling, vibrational IETS [9, 88] has been credited with enhancing the STM atomic resolution to chemical resolution, and now, magnetic IETS brings STM to magnetic resolution at the atomic scale.

Spurred by the experimental success and evolution, several new theoretical approaches emerged. Initially, the first theories were of perturbational character [72, 71] and explained the experimental scaling with the spin operator [29]. Beyond perturbation theories, two sudden-approximation ap-

proaches have been very successful. The first one deals with the complete atomic T-matrix [73] and explains the spin-operator dependence of the experimental data. The second one, uses the very large spin coupling to enforce the spin symmetries (value of the total spin, sum of the tunnelling electron spin and of the adsorbate spin) in the tunnelling process [22]. In this way, the excitation is seen as the sharing of the incident electron flux among all possible final channels, where the initial and final channels are connected via the formation of states of a well-defined total spin symmetry. In this way, the main features of the magnetic excitation process can be derived simply from spin coupling coefficients [22]

All of the above approaches are one-electron. These one-electron treatments are easy to implement using first-principles input and they generally yield quantitative data. However, many-body approaches are necessary when dealing with spin-flip dynamics. Indeed, Kondo-related physics has to be considered and this can have some important consequences on IETS such as the renormalization of the inelastic thresholds [140].

We foresee a lot of new developments in this field when atomic manipulation techniques are combined with magnetic IETS. On one side, new structures, tailored to exhibit special features [53, 85] in view of peculiar applications will be searched for. On the other side, dynamical studies of magnetic structures (e.g. direct study of the time evolution of a local magnetic moment) are already possible [38]. The combination of several techniques with magnetic IETS will surely give rise to new data and exciting applications. We think about noise studies combined with IETS [144] as well as resonance study with μ -wave probes [145, 146]. The ongoing development of the dynamical aspects of STM, together with all the know-how achieved these past years will further bring new exciting achievements in the field. These developments will prompt theoreticians to develop non-equilibrium techniques to treat the excitations with many body interactions taken into account, in parallel to the ever growing need for more quantitative, first-principles based calculations.

References

- [1] L. Esaki, New phenomenon in narrow germanium $p - n$ junctions, Phys. Rev. 109 (1958) 603–604. doi:10.1103/PhysRev.109.603.
URL <http://link.aps.org/doi/10.1103/PhysRev.109.603>

- [2] G. Binnig, H. Rohrer, C. Gerber, E. Weibel, Surface studies by scanning tunneling microscopy, *Phys. Rev. Lett.* 49 (1982) 57–61. doi:10.1103/PhysRevLett.49.57.
URL <http://link.aps.org/doi/10.1103/PhysRevLett.49.57>
- [3] B. Josephson, Possible new effects in superconductive tunnelling, *Physics Letters* 1 (7) (1962) 251 – 253.
doi:10.1016/0031-9163(62)91369-0.
URL <http://www.sciencedirect.com/science/article/pii/0031916362913690>
- [4] R. C. Jaklevic, J. Lambe, Molecular vibration spectra by electron tunneling, *Phys. Rev. Lett.* 17 (1966) 1139–1140.
doi:10.1103/PhysRevLett.17.1139.
URL <http://link.aps.org/doi/10.1103/PhysRevLett.17.1139>
- [5] P. Hansma, *Tunneling Spectroscopy*, Plenum, New York, 1982.
- [6] C. Petit, G. Salace, Inelastic electron tunneling spectrometer to characterize metal-oxide-semiconductor devices with ultrathin oxides, *Review of Scientific Instruments* 74 (2003) 4462–4467.
- [7] G. Binnig, N. Garcia, H. Rohrer, Conductivity sensitivity of inelastic scanning tunneling microscopy, *Phys. Rev. B* 32 (1985) 1336–1338. doi:10.1103/PhysRevB.32.1336.
URL <http://link.aps.org/doi/10.1103/PhysRevB.32.1336>
- [8] B. N. J. Persson, A. Baratoff, Inelastic electron tunneling from a metal tip: The contribution, *Phys. Rev. Lett.* 59 (1987) 339–342.
doi:10.1103/PhysRevLett.59.339.
URL <http://link.aps.org/doi/10.1103/PhysRevLett.59.339>
- [9] B. C. Stipe, M. A. Rezaei, W. Ho, Single-molecule vibrational spectroscopy and microscopy, *Science* 280 (5370) (1998) 1732–1735. doi:10.1126/science.280.5370.1732.
URL <http://www.sciencemag.org/content/280/5370/1732.abstract>
- [10] H. Ueba, Motions and reactions of single adsorbed molecules induced by vibrational excitation with stm, *Surface Review and Letters* 10 (5) (2003) 771–796.

- [11] T. Komeda, Chemical identification and manipulation of molecules by vibrational excitation
Progress in Surface Science 78 (2) (2005) 41 – 85.
doi:DOI:10.1016/j.progsurf.2005.05.001.
URL <http://www.sciencedirect.com/science/article/pii/S0079681605000262>
- [12] A. J. Heinrich, J. A. Gupta, C. P. Lutz, D. M. Eigler, Single-atom spin-flip spectroscopy, Science 306 (5695) (2004) 466–469.
doi:10.1126/science.1101077.
- [13] J. R. Hahn, H. J. Lee, W. Ho, Electronic resonance and symmetry in single-molecule inelastic electron tunneling,
Phys. Rev. Lett. 85 (2000) 1914–1917.
doi:10.1103/PhysRevLett.85.1914.
URL <http://link.aps.org/doi/10.1103/PhysRevLett.85.1914>
- [14] M. Alducin, D. Sánchez-Portal, A. Arnau, N. Lorente, Mixed-valency signature in vibrational inelastic electron tunneling spectroscopy,
Phys. Rev. Lett. 104 (2010) 136101.
doi:10.1103/PhysRevLett.104.136101.
URL <http://link.aps.org/doi/10.1103/PhysRevLett.104.136101>
- [15] N. Mingo, K. Makoshi, Calculation of the inelastic scanning tunneling image of acetylene on
Phys. Rev. Lett. 84 (2000) 3694–3697.
doi:10.1103/PhysRevLett.84.3694.
URL <http://link.aps.org/doi/10.1103/PhysRevLett.84.3694>
- [16] S. G. Tikhodeev, H. Ueba, Relation between inelastic electron tunneling and vibrational excitation,
Phys. Rev. B 70 (2004) 125414. doi:10.1103/PhysRevB.70.125414.
URL <http://link.aps.org/doi/10.1103/PhysRevB.70.125414>
- [17] N. Lorente, M. Persson, Theory of single molecule vibrational spectroscopy and microscopy,
Phys. Rev. Lett. 85 (2000) 2997–3000.
doi:10.1103/PhysRevLett.85.2997.
URL <http://link.aps.org/doi/10.1103/PhysRevLett.85.2997>
- [18] N. Lorente, Mode excitation induced by the scanning tunnelling microscope,
Applied Physics A: Materials Science & Processing 78 (2004) 799–806,
10.1007/s00339-003-2434-8.
URL <http://dx.doi.org/10.1007/s00339-003-2434-8>

- [19] S. Loth, K. von Bergmann, M. Termes, A. F. Otte, C. P. Lutz, A. J. Heinrich, Controlling the state of quantum spins with electric currents, *Nature Physics* 6 (2010) 340–344. doi:10.1038/nphys1616.
- [20] A. Troisi, J. Beebe, L. Picraux, R. van Zee, D. R. Stewart, M. A. Ratner, J. Kushmerick, Tracing electronic pathways in molecules by using inelastic tunneling spectroscopy, *PNAS* 104 (2007) 14255–14259.
- [21] M. Paulsson, T. Frederiksen, H. Ueba, N. Lorente, M. Brandbyge, Unified description of inelastic propensity rules for electron transport through nanoscale junctions, *Phys. Rev. Lett.* 100 (2008) 226604. doi:10.1103/PhysRevLett.100.226604. URL <http://link.aps.org/doi/10.1103/PhysRevLett.100.226604>
- [22] N. Lorente, J.-P. Gauyacq, Efficient spin transitions in inelastic electron tunneling spectroscopy, *Phys. Rev. Lett.* 103 (2009) 176601. doi:10.1103/PhysRevLett.103.176601. URL <http://link.aps.org/doi/10.1103/PhysRevLett.103.176601>
- [23] T. Balashov, A. F. Takács, W. Wulfhekel, J. Kirschner, Magnon excitation with spin-polarized scanning tunneling microscopy, *Phys. Rev. Lett.* 97 (18) (2006) 187201. doi:10.1103/PhysRevLett.97.187201.
- [24] A. A. Khajetoorians, S. Lounis, B. Chilian, A. T. Costa, L. Zhou, D. L. Mills, J. Wiebe, R. Wiesendanger, Itinerant nature of atom-magnetization excitation by tunneling electrons, *Phys. Rev. Lett.* 106 (3) (2011) 037205. doi:10.1103/PhysRevLett.106.037205.
- [25] S. Krause, L. Berbil-Bautista, G. Herzog, M. Bode, R. Wiesendanger, Current-induced magnetization switching with a spin-polarized scanning tunneling microscope, *Science* 317 (5844) (2007) 1537–1540. doi:10.1126/science.1145336.
- [26] G. Herzog, S. Krause, R. Wiesendanger, *Appl. Phys. Lett.* 96 (2010) 102505.
- [27] F. Delgado, J. J. Palacios, J. Fernández Rossier, Spin-transfer torque on a single magnetic adatom, *Phys. Rev. Lett.* 104 (2) (2010) 026601. doi:10.1103/PhysRevLett.104.026601.

- [28] F. D. Novaes, N. Lorente, J.-P. Gauyacq, Quenching of magnetic excitations in single adsorbates at surfaces: Mn on CuN/Cu(100), *Phys. Rev. B* 82 (15) (2010) 155401. doi:10.1103/PhysRevB.82.155401.
- [29] C. F. Hirjibehedin, C.-Y. Lin, A. F. Otte, M. Termes, C. P. Lutz, B. A. Jones, A. J. Heinrich, Large magnetic anisotropy of a single atomic spin embedded in a surface molecular network, *Science* 317 (5842) (2007) 1199–1203. doi:10.1126/science.1146110.
- [30] K. Yosida, *Theory of Magnetism*, Springer, Berlin, 1991.
- [31] N. Tsukahara, K.-I. Noto, M. Ohara, S. Shiraki, N. Takagi, Y. Takata, J. Miyawaki, M. Taguchi, A. Chainani, S. Shin, M. Kawai, Adsorption-induced switching of magnetic anisotropy in a single iron(II) phthalocyanine molecule on an oxidized Cu(110) surface, *Phys. Rev. Lett.* 102 (16) (2009) 167203. doi:10.1103/PhysRevLett.102.167203.
- [32] B. W. Dale, R. J. P. Williams, C. E. Johnson, T. L. Thorp, $S = 1$ spin state of divalent iron. i. magnetic properties of phthalocyanine iron (II), *J. Chem. Phys.* 49 (8) (1968) 3441–3444. doi:DOI:10.1063/1.1670617. URL <http://dx.doi.org/doi/10.1063/1.1670617>
- [33] B. W. Dale, R. J. P. Williams, P. R. Edwards, C. E. Johnson, $S = 1$ spin state of divalent iron. ii. a Mössbauer effect study of phthalocyanine iron (II), *J. Chem. Phys.* 49 (8) (1968) 3445–3449. doi:DOI:10.1063/1.1670618. URL <http://dx.doi.org/doi/10.1063/1.1670618>
- [34] J.-P. Gauyacq, F. D. Novaes, N. Lorente, Magnetic transitions induced by tunneling electrons in individual adsorbed *m*-phthalocyanine, *Phys. Rev. B* 81 (2010) 165423. doi:10.1103/PhysRevB.81.165423. URL <http://link.aps.org/doi/10.1103/PhysRevB.81.165423>
- [35] A. A. Khajetoorians, B. Chilian, J. Wiebe, S. Schwalow, F. Lechermann, R. Wiesendanger, Detecting excitation and magnetization of individual dopants in a semiconductor, *Nature* 467 (2010) 1084–1087. doi:10.1038/nature09519.
- [36] T. Balashov, T. Schuh, A. F. Takács, A. Ernst, S. Ostanin, J. Henk, I. Mertig, P. Bruno, T. Miyamachi, S. Suga, W. Wulfhchel,

- Magnetic anisotropy and magnetization dynamics of individual atoms and clusters of Fe and
 Phys. Rev. Lett. 102 (2009) 257203.
 doi:10.1103/PhysRevLett.102.257203.
 URL <http://link.aps.org/doi/10.1103/PhysRevLett.102.257203>
- [37] J. Fabian, S. D. Sarma, Spin relaxation of conduction electrons, J. Vac. Sc. Technol. B 17 (4) (1999) 1708–1715. doi:DOI:10.1116/1.590813.
 URL <http://dx.doi.org/doi/10.1116/1.590813>
- [38] S. Loth, M. Etzkorn, C. P. Lutz, D. M. Eigler, A. J. Heinrich, Measurement of fast electron spin relaxation times with atomic resolution, Science 329 (5999) (2010) 1628–1630. doi:10.1126/science.1191688.
 URL <http://www.sciencemag.org/content/329/5999/1628.abstract>
- [39] T. Schuh, T. Balashov, T. Miyamachi, A. F. Takacs, S. Suga, W. Wulfhekel, Lifetimes of magnetic excitations in Fe and Co atoms and clusters on Pt (111), Journal of Applied Physics 107 (2010) 09E156.
- [40] F. Meier, L. Zhou, J. Wiebe, R. Wiesendanger, Revealing magnetic interactions from single-atom magnetization curves, Science 320 (5872) (2008) 82–86. doi:10.1126/science.1154415.
 URL <http://www.sciencemag.org/content/320/5872/82.abstract>
- [41] T. Balashov, A. F. Takács, M. Däne, A. Ernst, P. Bruno, W. Wulfhekel, Inelastic electron-magnon interaction and spin transfer torque, Phys. Rev. B 78 (2008) 174404. doi:10.1103/PhysRevB.78.174404.
 URL <http://link.aps.org/doi/10.1103/PhysRevB.78.174404>
- [42] C. L. Gao, A. Ernst, G. Fischer, W. Hergert, P. Bruno, W. Wulfhekel, J. Kirschner, Spin wave dispersion on the nanometer scale, Phys. Rev. Lett. 101 (2008) 167201. doi:10.1103/PhysRevLett.101.167201.
 URL <http://link.aps.org/doi/10.1103/PhysRevLett.101.167201>
- [43] C. F. Hirjibeheding, C. P. Lutz, A. J. Heinrich, Spin Coupling in engineered atomic structures, Science 312 (5776) (2006) 1021–1024. doi:10.1126/science.1125398.
- [44] J. P. Gauyacq, N. Lorente, Excitation of spin waves by tunneling electrons in ferromagnetic and antiferromagnetic spin- $\frac{1}{2}$ Heisenberg chains, Phys. Rev. B 83 (3) (2011) 035418. doi:10.1103/PhysRevB.83.035418.

- [45] A. N. Rudenko, V. V. Mazurenko, V. I. Anisimov, A. I. Lichtenstein, Weak ferromagnetism in Mn nanochains on the CuN surface, *Phys. Rev. B* 79 (2009) 144418. doi:10.1103/PhysRevB.79.144418. URL <http://link.aps.org/doi/10.1103/PhysRevB.79.144418>
- [46] X. Chen, Y.-S. Fu, S.-H. Ji, T. Zhang, P. Cheng, X.-C. Ma, X.-L. Zou, W.-H. Duan, J.-F. Jia, Q.-K. Xue, Probing superexchange interaction in molecular magnets by spin-flip spectroscopy and microscopy, *Phys. Rev. Lett.* 101 (19) (2008) 197208. doi:10.1103/PhysRevLett.101.197208.
- [47] A. F. Otte, M. Ternes, K. von Bergmann, S. Loth, C. P. Lutz, C. F. Hirjibehedin, A. J. Heinrich, The role of magnetic anisotropy in the Kondo effect, *Nature Physics* 4 (2008) 847–850.
- [48] N. Knorr, M. A. Schneider, L. Diekhöner, P. Wahl, K. Kern, Kondo effect of single Co adatoms on Cu surfaces, *Phys. Rev. Lett.* 88 (2002) 096804. doi:10.1103/PhysRevLett.88.096804. URL <http://link.aps.org/doi/10.1103/PhysRevLett.88.096804>
- [49] A. Hurley, N. Baadji, S. Sanvito, Perturbative approach to the Kondo effect in magnetic atoms on nonmagnetic substrates, *Phys. Rev. B* 84 (2011) 115435. doi:10.1103/PhysRevB.84.115435.
- [50] J. Paaske, A. Rosch, P. Wolfle, N. Mason, C. M. Marcus, J. Nygard, Non-equilibrium singlet-triplet Kondo effect in carbon nanotubes, *Nat. Phys.* 2 (2) (2006) 460 – 464.
- [51] N. Roch, S. Florens, V. Bouchiat, W. Wernsdorfer, F. Balestro, Quantum phase transition in a single-molecule quantum dot, *Nature* 453 (2008) 633–637.
- [52] J. J. Parks, A. R. Champagne, T. A. Costi, W. W. Shum, A. N. Pasupathy, E. Neuscamman, S. Flores-Torres, P. S. Cornaglia, A. A. Aligia, C. A. Balseiro, G. K.-L. Chan, H. D. Abrua, D. C. Ralph, Mechanical Control of spin states in spin-1 molecules and the underscreened Kondo effect, *Science* 328 (5984) (2010) 1370–1373. doi:10.1126/science.1186874.
- [53] A. F. Otte, M. Ternes, S. Loth, C. P. Lutz, C. F. Hirjibehedin, A. J. Heinrich,

- Spin excitations of a Kondo-screened atom Coupled to a second magnetic atom,
 Phys. Rev. Lett. 103 (2009) 107203.
 doi:10.1103/PhysRevLett.103.107203.
 URL <http://link.aps.org/doi/10.1103/PhysRevLett.103.107203>
- [54] G. Autès, C. Barreteau, D. Spanjaard, M.-C. Desjonquères,
 Magnetism of iron: from the bulk to the monatomic wire, Journal of
 Physics: Condensed Matter 18 (29) (2006) 6785.
 URL <http://stacks.iop.org/0953-8984/18/i=29/a=018>
- [55] M.-C. Desjonquères, C. Barreteau, G. Autès, D. Spanjaard,
 Orbital contribution to the magnetic properties of iron as a function of dimensionality,
 Phys. Rev. B 76 (2007) 024412. doi:10.1103/PhysRevB.76.024412.
 URL <http://link.aps.org/doi/10.1103/PhysRevB.76.024412>
- [56] P. Bruno, Tight-binding approach to the orbital magnetic moment and magnetocrystalline a
 Phys. Rev. B 39 (1989) 865–868. doi:10.1103/PhysRevB.39.865.
 URL <http://link.aps.org/doi/10.1103/PhysRevB.39.865>
- [57] P. Błoński, J. Hafner, Magnetic anisotropy of transition-metal dimers: Density functional cal
 Phys. Rev. B 79 (2009) 224418. doi:10.1103/PhysRevB.79.224418.
 URL <http://link.aps.org/doi/10.1103/PhysRevB.79.224418>
- [58] A. B. Shick, F. Máca, A. I. Lichtenstein,
 Magnetic anisotropy of single 3d spins on a CuN surface, Phys.
 Rev. B 79 (2009) 172409. doi:10.1103/PhysRevB.79.172409.
 URL <http://link.aps.org/doi/10.1103/PhysRevB.79.172409>
- [59] O. Šipr, S. Bornemann, J. Minár, H. Ebert,
 Magnetic anisotropy of Fe and Co adatoms and monolayers: Need for a proper treatment of
 Phys. Rev. B 82 (2010) 174414. doi:10.1103/PhysRevB.82.174414.
 URL <http://link.aps.org/doi/10.1103/PhysRevB.82.174414>
- [60] A. B. Shick, F. Máca, M. Ondráček, O. N. Mryasov, T. Jungwirth,
 Large magnetic anisotropy and tunneling anisotropic magnetoresistance in layered bimetallic
 Phys. Rev. B 78 (2008) 054413. doi:10.1103/PhysRevB.78.054413.
 URL <http://link.aps.org/doi/10.1103/PhysRevB.78.054413>
- [61] P. Błoński, A. Lehnert, S. Dennler, S. Rusponi, M. Etzkorn,
 G. Moulas, P. Bencok, P. Gambardella, H. Brune, J. Hafner,

- Magnetocrystalline anisotropy energy of Co and Fe adatoms on the (111) surfaces of pd and
 Phys. Rev. B 81 (2010) 104426. doi:10.1103/PhysRevB.81.104426.
 URL <http://link.aps.org/doi/10.1103/PhysRevB.81.104426>
- [62] M. A. Barral, P. Roura-Bas, A. M. Llois, A. A. Aligia,
 Kondo behavior of anisotropic single atomic spins on a Cu₂N molecular layer,
 Phys. Rev. B 82 (2010) 125438. doi:10.1103/PhysRevB.82.125438.
 URL <http://link.aps.org/doi/10.1103/PhysRevB.82.125438>
- [63] J. Wang, Y. Shi, J. Cao, R. Wu,
 Magnetization and magnetic anisotropy of metallophthalocyanine molecules from the first p
 Applied Physics Letters 94 (12) (2009) 122502.
 doi:DOI:10.1063/1.3100783.
 URL <http://dx.doi.org/doi/10.1063/1.3100783>
- [64] A. Al-Zubi, G. Bihlmayer, S. Blügel,
 Magnetism of 3d transition-metal monolayers on Rh(100), Phys.
 Rev. B 83 (2011) 024407. doi:10.1103/PhysRevB.83.024407.
 URL <http://link.aps.org/doi/10.1103/PhysRevB.83.024407>
- [65] P. Błoński, J. Hafner, Density-functional theory of the magnetic anisotropy of nanostructures
 Journal of Physics: Condensed Matter 21 (42) (2009) 426001.
 URL <http://stacks.iop.org/0953-8984/21/i=42/a=426001>
- [66] L. Fernández Seivane, J. Ferrer, Magnetic anisotropies of late transition metal atomic clusters
 Phys. Rev. Lett. 99 (2007) 183401.
 doi:10.1103/PhysRevLett.99.183401.
 URL <http://link.aps.org/doi/10.1103/PhysRevLett.99.183401>
- [67] H. Zhang, M. Richter, K. Koepf, I. Opahle, Ferenc Tasndi, H. Eschrig,
 Electric-field control of surface magnetic anisotropy: a density functional approach,
 New Journal of Physics 11 (4) (2009) 043007.
 URL <http://stacks.iop.org/1367-2630/11/i=4/a=043007>
- [68] J. Kuneš, P. Novák, R. Schmid, P. Blaha, K. Schwarz,
 Electronic structure of fcc th: Spin-orbit calculation with 6p_{1/2} local orbital extension,
 Phys. Rev. B 64 (2001) 153102. doi:10.1103/PhysRevB.64.153102.
 URL <http://link.aps.org/doi/10.1103/PhysRevB.64.153102>

- [69] S. Loth, C. P. Lutz, A. J. Heinrich, Spin-polarized spin excitation spectroscopy, *New Journal of Physics* 12 (12) (2010) 125021.
URL <http://stacks.iop.org/1367-2630/12/i=12/a=125021>
- [70] B. Chilian, A. A. Khajetoorians, J. Wiebe, R. Wiesendanger, Experimental variation and theoretical analysis of the inelastic contribution to atomic spin Hall effect, *Phys. Rev. B* 83 (2011) 195431. doi:10.1103/PhysRevB.83.195431.
URL <http://link.aps.org/doi/10.1103/PhysRevB.83.195431>
- [71] J. Fernández Rossier, Theory of single-spin inelastic tunneling spectroscopy, *Phys. Rev. Lett.* 102 (2009) 256802.
doi:10.1103/PhysRevLett.102.256802.
URL <http://link.aps.org/doi/10.1103/PhysRevLett.102.256802>
- [72] J. Fransson, Spin inelastic electron tunneling spectroscopy on local spin adsorbed on surface, *Nano Letters* 9 (6) (2009) 2414–2417, pMID: 19507889.
doi:10.1021/nl901066a.
URL <http://pubs.acs.org/doi/abs/10.1021/nl901066a>
- [73] M. Persson, Theory of inelastic electron tunneling from a localized spin in the impulsive approximation, *Phys. Rev. Lett.* 103 (2009) 050801.
doi:10.1103/PhysRevLett.103.050801.
URL <http://link.aps.org/doi/10.1103/PhysRevLett.103.050801>
- [74] J. Tersoff, D. R. Hamann, Theory and application for the scanning tunneling microscope, *Phys. Rev. Lett.* 50 (1983) 1998–2001.
doi:10.1103/PhysRevLett.50.1998.
URL <http://link.aps.org/doi/10.1103/PhysRevLett.50.1998>
- [75] J. M. Soler, E. Artacho, J. D. Gale, A. García, J. Junquera, P. Ordejón, D. Sánchez-Portal, The siesta method for ab initio order-N materials simulation, *Journal of Physics: Condensed Matter* 14 (11) (2002) 2745.
URL <http://stacks.iop.org/0953-8984/14/i=11/a=302>
- [76] X. Lu, K. W. Hipps, Scanning tunneling microscopy of metal phthalocyanines: d⁶ and d⁸ cases, *The Journal of Physical Chemistry B* 101 (27) (1997) 5391–5396.
doi:10.1021/jp9707448.
URL <http://pubs.acs.org/doi/abs/10.1021/jp9707448>

- [77] M.-S. Liao, S. Scheiner, Electronic structure and bonding in metal phthalocyanines, metal=Fe, *J. Chem. Phys.* 114 (22) (2001) 9780–9791. doi:DOI:10.1063/1.1367374. URL <http://dx.doi.org/doi/10.1063/1.1367374>
- [78] N. Marom, L. Kronik, Density functional theory of transition metal phthalocyanines, II: electronic transport, *Applied Physics A: Materials Science and Processing* 95 (2009) 165–172, 10.1007/s00339-008-5005-1. URL <http://dx.doi.org/10.1007/s00339-008-5005-1>
- [79] M. Brandbyge, J.-L. Mozos, P. Ordejón, J. Taylor, K. Stokbro, Density-functional method for nonequilibrium electron transport, *Phys. Rev. B* 65 (2002) 165401. doi:10.1103/PhysRevB.65.165401. URL <http://link.aps.org/doi/10.1103/PhysRevB.65.165401>
- [80] F. D. Novaes, A. A. J. R. d. Silva, A. Fazzio, Density functional theory method for non-equilibrium charge transport calculations: TRANSAMPA, *Brazilian Journal of Physics* 36 (2006) 799 – 807.
- [81] T. Frederiksen, M. Paulsson, M. Brandbyge, A.-P. Jauho, Inelastic transport theory from first principles: Methodology and application to nanoscale devices, *Phys. Rev. B* 75 (2007) 205413. doi:10.1103/PhysRevB.75.205413. URL <http://link.aps.org/doi/10.1103/PhysRevB.75.205413>
- [82] M. Paulsson, M. Brandbyge, Transmission eigenchannels from nonequilibrium green’s function method, *Phys. Rev. B* 76 (2007) 115117. doi:10.1103/PhysRevB.76.115117. URL <http://link.aps.org/doi/10.1103/PhysRevB.76.115117>
- [83] Y. Yayon, V. W. Brar, L. Senapati, S. C. Erwin, M. F. Crommie, Observing spin polarization of individual magnetic adatoms, *Phys. Rev. Lett.* 99 (2007) 067202. doi:10.1103/PhysRevLett.99.067202. URL <http://link.aps.org/doi/10.1103/PhysRevLett.99.067202>
- [84] C. Iacovita, M. V. Rastei, B. W. Heinrich, T. Brumme, J. Kortus, L. Limot, J. P. Bucher, Visualizing the spin of individual cobalt-phthalocyanine molecules, *Phys. Rev. Lett.* 101 (2008) 116602. doi:10.1103/PhysRevLett.101.116602. URL <http://link.aps.org/doi/10.1103/PhysRevLett.101.116602>

- [85] A. A. Khajetoorians, J. Wiebe, B. Chilian, R. Wiesendanger, Realizing all-spin based logic operations atom by atom, *Science* 332 (6033) (2011) 1062–1064. doi:10.1126/science.1201725. URL <http://www.sciencemag.org/content/332/6033/1062.abstract>
- [86] L. Zhou, F. Meier, J. Wiebe, R. Wiesendanger, Inversion of spin polarization above individual magnetic adatoms, *Phys. Rev. B* 82 (2010) 012409. doi:10.1103/PhysRevB.82.012409. URL <http://link.aps.org/doi/10.1103/PhysRevB.82.012409>
- [87] D. Sarrate, P. Ferriani, Y. Yoshida, S.-W. Hla, M. Menzel, K. von Bergmann, S. Heinze, A. Kubetzka, R. Wiesendanger, Imaging and manipulating the spin direction of individual atoms, *Nature Nanotech.* 5 (2010) 350.
- [88] W. Ho, Single-molecule chemistry, *J. Chem. Phys.* 117 (24) (2002) 11033–11061. doi:DOI:10.1063/1.1521153. URL <http://dx.doi.org/doi/10.1063/1.1521153>
- [89] R. A. Abram, A. Herzenberg, Rotational excitation of H₂ by slow electrons, *Chemical Physics Letters* 3 (1969) 187 – 190.
- [90] G. J. Schulz, Resonances in electron impact on diatomic molecules, *Rev. Mod. Phys.* 45 (1973) 423–486. doi:10.1103/RevModPhys.45.423. URL <http://link.aps.org/doi/10.1103/RevModPhys.45.423>
- [91] D. Teillet-Billy, J. P. Gauyacq, M. Persson, Molecular rotation induced by inelastic electron tunneling, *Phys. Rev. B* 62 (2000) R13306–R13309. doi:10.1103/PhysRevB.62.R13306. URL <http://link.aps.org/doi/10.1103/PhysRevB.62.R13306>
- [92] B. C. Stipe, M. A. Rezaei, W. Ho, Inducing and viewing the rotational motion of a single molecule, *Science* 279 (5358) (1998) 1907–1909. doi:10.1126/science.279.5358.1907. URL <http://www.sciencemag.org/content/279/5358/1907.abstract>
- [93] D. Teillet-Billy, L. Malegat, J. P. Gauyacq, Electronic excitation as a resonant process: e - O₂ collisions, *Journal*

of Physics B: Atomic and Molecular Physics 20 (13) (1987) 3201.
URL <http://stacks.iop.org/0022-3700/20/i=13/a=026>

- [94] B. Bahrim, D. Teillet-Billy, J. P. Gauyacq, O⁻ ions in front of a metal surface: Application to an oxygen singlet quenching process, Phys. Rev. B 50 (1994) 7860–7867. doi:10.1103/PhysRevB.50.7860.
URL <http://link.aps.org/doi/10.1103/PhysRevB.50.7860>
- [95] B. Bahrim, D. Teillet-Billy, J. Gauyacq, Ionization probabilities of oxygen sputtered from metal surfaces, Surface Science 316 (1-2) (1994) 189. doi:10.1016/0039-6028(94)91139-8.
URL <http://www.sciencedirect.com/science/article/pii/0039602894911398>
- [96] M. Allan, Transitions between the $^2\pi_{1/2}$ and $^2\pi_{3/2}$ spin-orbit Components of NO induced by Phys. Rev. Lett. 93 (2004) 063201. doi:10.1103/PhysRevLett.93.063201.
URL <http://link.aps.org/doi/10.1103/PhysRevLett.93.063201>
- [97] M. Allan, Electron collisions with NO: elastic scattering, vibrational excitation and $^2\pi_{1/2}$ and Journal of Physics B: Atomic, Molecular and Optical Physics 38 (5) (2005) 603.
URL <http://stacks.iop.org/0953-4075/38/i=5/a=011>
- [98] J. W. Gadzuk, Shape resonances, overtones, and electron energy loss spectroscopy of gas phase J. Chem. Phys. 79 (8) (1983) 3982–3987. doi:DOI:10.1063/1.446266.
URL <http://dx.doi.org/doi/10.1063/1.446266>
- [99] R. E. Palmer, P. J. Rous, Resonances in electron scattering by molecules on surfaces, Rev. Mod. Phys. 64 (1992) 383–440. doi:10.1103/RevModPhys.64.383.
URL <http://link.aps.org/doi/10.1103/RevModPhys.64.383>
- [100] V. Djamo, D. Teillet-Billy, J. P. Gauyacq, Resonant vibrational excitation of adsorbed molecules by electron impact, Phys. Rev. Lett. 71 (1993) 3267–3270. doi:10.1103/PhysRevLett.71.3267.
URL <http://link.aps.org/doi/10.1103/PhysRevLett.71.3267>
- [101] F. Delgado, J. Fernández Rossier, Spin dynamics of current-driven single magnetic adatoms and molecules,

- Phys. Rev. B 82 (2010) 134414. doi:10.1103/PhysRevB.82.134414.
 URL <http://link.aps.org/doi/10.1103/PhysRevB.82.134414>
- [102] N. Lorente, Dynamics, Handbook of Surface Science, edited by E. Hasselbrink and B. I. Lundqvist, North Holland, Amsterdam, 2008.
- [103] J. D. McNeill, R. L. Lingle, R. E. Jordan, D. F. Padowitz, C. B. Harris, Interfacial quantum well states of Xe and Kr adsorbed on Ag(111), J. Chem. Phys. 105 (9) (1996) 3883–3891. doi:DOI:10.1063/1.472209.
 URL <http://dx.doi.org/doi/10.1063/1.472209>
- [104] M. Wolf, E. Knoesel, T. Hertel, Ultrafast dynamics of electrons in image-potential states on clean and Xe-covered Cu(111), Phys. Rev. B 54 (1996) R5295–R5298.
 doi:10.1103/PhysRevB.54.R5295.
 URL <http://link.aps.org/doi/10.1103/PhysRevB.54.R5295>
- [105] D. C. Marinica, C. Ramseyer, A. G. Borisov, D. Teillet-Billy, J. P. Gauyacq, W. Berthold, P. Feulner, U. Höfer, Effect of an atomically thin dielectric film on the surface electron dynamics: Image-potential, Phys. Rev. Lett. 89 (2002) 046802.
 doi:10.1103/PhysRevLett.89.046802.
 URL <http://link.aps.org/doi/10.1103/PhysRevLett.89.046802>
- [106] W. Wurth, D. Menzel, Ultrafast electron dynamics at surfaces probed by resonant auger spectroscopy, Chemical Physics 251 (1-3) (2000) 141 – 149.
 doi:10.1016/S0301-0104(99)00305-5.
 URL <http://www.sciencedirect.com/science/article/pii/S0301010499003055>
- [107] J. P. Gauyacq, A. G. Borisov, Excited electron transfer between a core-excited $\text{Ar}^*(2p^{-1}4s)$ and a surface, Phys. Rev. B 69 (2004) 235408. doi:10.1103/PhysRevB.69.235408.
 URL <http://link.aps.org/doi/10.1103/PhysRevB.69.235408>
- [108] D. E. Freedman, W. H. Harman, T. D. Harris, G. J. Long, C. J. Chang, J. R. Long, Slow magnetic relaxation in a high-spin iron(II) Complex, Journal of the American Chemical Society 132 (4) (2010) 1224–1225, PMID: 20055389. doi:10.1021/ja909560d.
 URL <http://pubs.acs.org/doi/abs/10.1021/ja909560d>

- [109] R. B. Muniz, D. L. Mills, Local spin dynamics of magnetic moments on metal surfaces, Phys. Rev. B 68 (2003) 224414. doi:10.1103/PhysRevB.68.224414.
URL <http://link.aps.org/doi/10.1103/PhysRevB.68.224414>
- [110] S. Lounis, A. T. Costa, R. B. Muniz, D. L. Mills, Dynamical magnetic excitations of nanostructures from first principles, Phys. Rev. Lett. 105 (2010) 187205. doi:10.1103/PhysRevLett.105.187205.
URL <http://link.aps.org/doi/10.1103/PhysRevLett.105.187205>
- [111] S. Lounis, A. T. Costa, R. B. Muniz, D. L. Mills, Theory of local dynamical magnetic susceptibilities from the Korringa-Kohn-Rostoker green Phys. Rev. B 83 (2011) 035109. doi:10.1103/PhysRevB.83.035109.
URL <http://link.aps.org/doi/10.1103/PhysRevB.83.035109>
- [112] J. des Cloizeaux, J. J. Pearson, Spin-wave spectrum of the antiferromagnetic linear chain, Phys. Rev. 128 (1962) 2131–2135. doi:10.1103/PhysRev.128.2131.
URL <http://link.aps.org/doi/10.1103/PhysRev.128.2131>
- [113] R. Orbach, Antiferromagnetic magnon dispersion law and Bloch wall energies in ferromagnets Phys. Rev. 115 (1959) 1181–1184. doi:10.1103/PhysRev.115.1181.
URL <http://link.aps.org/doi/10.1103/PhysRev.115.1181>
- [114] L. F. Mattheiss, Antiferromagnetic linear chain, Phys. Rev. 123 (1961) 1209–1218. doi:10.1103/PhysRev.123.1209.
URL <http://link.aps.org/doi/10.1103/PhysRev.123.1209>
- [115] N. Ashcroft, M. N.D., Solid State Physics, HRW International Editions, Philadelphia, 1976.
- [116] M. Karbach, G. Müller, A. H. Bougourzi, A. Fledderjohann, K.-H. Mütter, Two-spinon dynamic structure factor of the one-dimensional Heisenberg antiferromagnet Phys. Rev. B 55 (1997) 12510–12517. doi:10.1103/PhysRevB.55.12510.
URL <http://link.aps.org/doi/10.1103/PhysRevB.55.12510>
- [117] M. Karbach, G. Müller, Line-shape predictions via Bethe ansatz for the one-dimensional spin-1 chain Phys. Rev. B 62 (2000) 14871–14879. doi:10.1103/PhysRevB.62.14871.
URL <http://link.aps.org/doi/10.1103/PhysRevB.62.14871>

- [118] J. P. Gauyacq, N. Lorente, Magnetic excitation by tunneling electrons of frustrated ferromagnetic chain, Phys. Rev. B 84 (2011) 085415. doi:10.1103/PhysRevB.84.085415.
URL <http://link.aps.org/doi/10.1103/PhysRevB.84.085415>
- [119] T. Hikihara, L. Kecke, T. Momoi, A. Furusaki, Vector chiral and multipolar orders in the spin- $\frac{1}{2}$ frustrated ferromagnetic chain in magnetic field, Phys. Rev. B 78 (2008) 144404. doi:10.1103/PhysRevB.78.144404.
URL <http://link.aps.org/doi/10.1103/PhysRevB.78.144404>
- [120] J. Sudan, A. Lüscher, A. M. Läuchli, Emergent multipolar spin correlations in a fluctuating spiral: The frustrated ferromagnetic chain, Phys. Rev. B 80 (2009) 140402. doi:10.1103/PhysRevB.80.140402.
URL <http://link.aps.org/doi/10.1103/PhysRevB.80.140402>
- [121] L. Kecke, T. Momoi, A. Furusaki, Multimagnon bound states in the frustrated ferromagnetic one-dimensional chain, Phys. Rev. B 76 (2007) 060407. doi:10.1103/PhysRevB.76.060407.
URL <http://link.aps.org/doi/10.1103/PhysRevB.76.060407>
- [122] T. Vekua, A. Honecker, H.-J. Mikeska, F. Heidrich-Meisner, Correlation functions and excitation spectrum of the frustrated ferromagnetic spin- $\frac{1}{2}$ chain in magnetic field, Phys. Rev. B 76 (2007) 174420. doi:10.1103/PhysRevB.76.174420.
URL <http://link.aps.org/doi/10.1103/PhysRevB.76.174420>
- [123] A. V. Chubukov, Chiral, nematic, and dimer states in quantum spin chains, Phys. Rev. B 44 (1991) 4693–4696. doi:10.1103/PhysRevB.44.4693.
URL <http://link.aps.org/doi/10.1103/PhysRevB.44.4693>
- [124] M. Hase, H. Kuroe, K. Ozawa, O. Suzuki, H. Kitazawa, G. Kido, T. Sekine, Magnetic properties of $\text{Rb}_2\text{Cu}_2\text{Mo}_3\text{O}_{12}$ including a one-dimensional spin-1/2 Heisenberg system, Phys. Rev. B 70 (2004) 104426. doi:10.1103/PhysRevB.70.104426.
URL <http://link.aps.org/doi/10.1103/PhysRevB.70.104426>
- [125] S.-L. Drechsler, O. Volkova, A. N. Vasiliev, N. Tristan, J. Richter, M. Schmitt, H. Rosner, J. Málek, R. Klingeler, A. A. Zvyagin, B. Büchner, Frustrated Cuprate route from antiferromagnetic to Ferromagnetic spin- $\frac{1}{2}$ Heisenberg chains, Phys. Rev. Lett. 98 (2007) 077202.

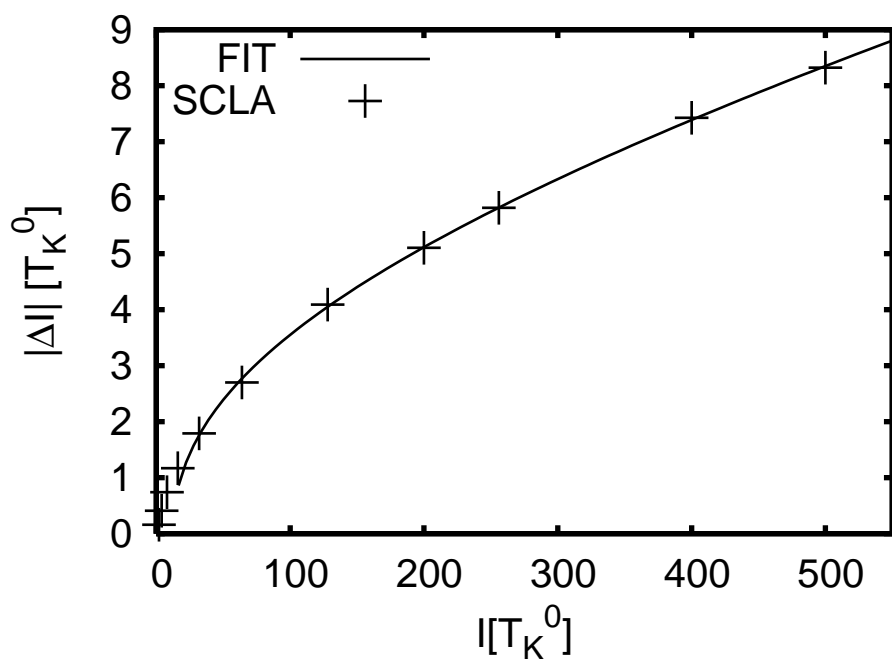
doi:10.1103/PhysRevLett.98.077202.

URL <http://link.aps.org/doi/10.1103/PhysRevLett.98.077202>

- [126] M. G. Banks, R. K. Kremer, C. Hoch, A. Simon, B. Oulad-diaf, J.-M. Broto, H. Rakoto, C. Lee, M.-H. Whangbo, Magnetic ordering in the frustrated Heisenberg chain system cupric chloride CuCl_2 , Phys. Rev. B 80 (2009) 024404. doi:10.1103/PhysRevB.80.024404. URL <http://link.aps.org/doi/10.1103/PhysRevB.80.024404>
- [127] A. A. Tsirlin, R. Nath, J. Sichelschmidt, Y. Skourski, C. Geibel, H. Rosner, Frustrated couplings between alternating spin- $\frac{1}{2}$ chains in AgVOAsO_4 , Phys. Rev. B 83 (2011) 144412. doi:10.1103/PhysRevB.83.144412. URL <http://link.aps.org/doi/10.1103/PhysRevB.83.144412>
- [128] J. Kondo, Resistance minimum in dilute magnetic alloys, Progress of Theoretical Physics 32 (1) (1964) 37–49. doi:10.1143/PTP.32.37. URL <http://ptp.ipap.jp/link?PTP/32/37/>
- [129] V. Madhavan, W. Chen, T. Jamneala, M. F. Crommie, N. S. Wingreen, Tunneling into a single magnetic atom: Spectroscopic evidence of the Kondo resonance, Science 280 (5363) (1998) 567–569. doi:10.1126/science.280.5363.567. URL <http://www.sciencemag.org/content/280/5363/567.abstract>
- [130] J. Li, W.-D. Schneider, R. Berndt, B. Delley, Kondo scattering observed at a single magnetic impurity, Phys. Rev. Lett. 80 (1998) 2893–2896. doi:10.1103/PhysRevLett.80.2893. URL <http://link.aps.org/doi/10.1103/PhysRevLett.80.2893>
- [131] M. Ternes, A. J. Heinrich, W.-D. Schneider, Spectroscopic manifestations of the Kondo effect on single adatoms, Journal of Physics: Condensed Matter 21 (5) (2009) 053001. URL <http://stacks.iop.org/0953-8984/21/i=5/a=053001>
- [132] A. C. Hewson, The Kondo Problem to Heavy Fermions, Cambridge studies in magnetism, Cambridge University Press, 1993.
- [133] P. Fulde, Electron correlations in molecules and solids, Solid-state sciences, Springer Verlag, 1995.

- [134] R. Korytár, Nicolás Lorente, Multi-orbital non-crossing approximation from maximally localized wannier functions: the Kondo signature of copper phthalocyanine on Ag(100), *Journal of Physics: Condensed Matter* 23 (35) (2011) 355009.
- [135] K. Nagaoka, T. Jamneala, M. Grobis, M. F. Crommie, Temperature dependence of a single Kondo impurity, *Phys. Rev. Lett.* 88 (2002) 077205. doi:10.1103/PhysRevLett.88.077205.
URL <http://link.aps.org/doi/10.1103/PhysRevLett.88.077205>
- [136] V. Madhavan, W. Chen, T. Jamneala, M. F. Crommie, N. S. Wingreen, Local spectroscopy of a Kondo impurity: Co on Au(111), *Phys. Rev. B* 64 (2001) 165412. doi:10.1103/PhysRevB.64.165412.
URL <http://link.aps.org/doi/10.1103/PhysRevB.64.165412>
- [137] G. Zaránd, L. Borda, J. von Delft, N. Andrei, Theory of inelastic scattering from magnetic impurities, *Phys. Rev. Lett.* 93 (2004) 107204. doi:10.1103/PhysRevLett.93.107204.
URL <http://link.aps.org/doi/10.1103/PhysRevLett.93.107204>
- [138] L. Borda, L. Fritz, N. Andrei, G. Zaránd, Theory of inelastic scattering from quantum impurities, *Phys. Rev. B* 75 (2007) 235112. doi:10.1103/PhysRevB.75.235112.
URL <http://link.aps.org/doi/10.1103/PhysRevB.75.235112>
- [139] R. Zitko, T. Pruschke, Many-particle effects in adsorbed magnetic atoms with easy-axis anisotropy: the case of Fe on CuN/Cu(100) surface, *New Journal of Physics* 12 (12) (2010) 063040.
- [140] R. Korytár, N. Lorente, J.-P. Gauyacq, Many-body effects in magnetic inelastic electron tunneling spectroscopy, *Phys. Rev. B* 85 (2012) 125434. doi:10.1103/PhysRevB.85.125434.
URL <http://link.aps.org/doi/10.1103/PhysRevB.85.125434>
- [141] A. Mugarza, C. Krull, R. Robles, S. Stepanow, G. Ceballos, P. Gambardella, Spin coupling and relaxation inside molecule metal contacts, *Nat. Comm.* 2 (2011) 490.
- [142] J. E. Moore, X.-G. Wen, Anomalous magnetic splitting of the Kondo resonance, *Phys. Rev. Lett.* 85 (8) (2000) 1722–1725. doi:10.1103/PhysRevLett.85.1722.

- [143] A. Rosch, T. A. Costi, J. Paaske, P. Wölfle, Spectral function of the Kondo model in high magnetic fields, *Phys. Rev. B* 68 (1) (2003) 014430. doi:10.1103/PhysRevB.68.014430.
- [144] J. Schaffert, M. C. Cottin, A. Sonntag, H. Karacuban, C. A. Bobisch, N. Lorente, J.-P. Gauyacq, R. Möller, unpublished.
- [145] T. Komeda, Y. Manassen, Distribution of frequencies of a single precessing spin detected by scanning tunneling microscope, *Applied Physics Letters* 92 (2008) 212506.
- [146] A. V. Balatsky, J. Fransson, D. Mozyrsky, Y. Manassen, STM NMR and nuclear spin noise, *Phys. Rev. B* 73 (2006) 184429. doi:10.1103/PhysRevB.73.184429. URL <http://link.aps.org/doi/10.1103/PhysRevB.73.184429>



Abstract

Keywords:

1.

